Long Time Series Measurements of Munitions Mobility in the Wave-Current Boundary Layer

SERDP Project Number 2320

U.S. Naval Research Laboratory, Stennis Space Center, MS
Joseph Calantoni

University of Florida, Gainesville, FL
Tracy Staples & Alexandru Sheremet

18 March 2014

REPORT DOCUMENTATION PAGE

Form Approved
OMB No. 0704-0188

1. REPORT DATE *(DD-MM-YYYY)*	2. REPORT TYPE	3. DATES COVERED *(From - To)*
02/18/2014	SERDP Interim Report	

4. TITLE AND SUBTITLE
Long Time Series Measurements of Munitions Mobility in the Wave-Current Boundary Layer

5a. CONTRACT NUMBER

5b. GRANT NUMBER

5c. PROGRAM ELEMENT NUMBER

6. AUTHOR(S)
Joseph Calantoni, NRL

Tracy Staples
Alexandru Sheremet
University of Florida, Gainesville

5d. PROJECT NUMBER
MR-2320

5e. TASK NUMBER

5f. WORK UNIT NUMBER

7. PERFORMING ORGANIZATION NAME(S) AND ADDRESS(ES)
U.S. Naval Research Laboratory
1005 Balch Blvd, Room D-17D, Code 7434 Stennis Space Center, MS 39529

8. PERFORMING ORGANIZATION REPORT NUMBER
MR-2320

9. SPONSORING/MONITORING AGENCY NAME(S) AND ADDRESS(ES)
Strategic Environmental Research and Development Program
4800 Mark Center Drive, Suite 17D03
Alexandria, VA 22350-3605

10. SPONSOR/MONITOR'S ACRONYM(S)
SERDP

11. SPONSOR/MONITOR'S REPORT NUMBER(S)
MR-2320

12. DISTRIBUTION/AVAILABILITY STATEMENT
Distribution A; Approved for public release: Distribution unlimited.

13. SUPPLEMENTARY NOTES

14. ABSTRACT

The objective of this report was to provide detailed time series measurements of the in situ boundary layer processes responsible for munitions mobility including transport, burial, and excavation. The researchers performed the first of a proposed set of field experiments to characterize the environment in which munitions are found while simultaneously recording the location of munitions relative to the seafloor at high spatial and temporal frequency. Unlike previous investigations that have provided before and after snapshots of munitions mobility, our instrumentation is capable of providing high spatial and temporal resolution measurements of all the relevant boundary layer processes (e.g., wave height and direction, current profiles, suspended sediment concentration, and sediment erosion and deposition) while simultaneously monitoring the mobility of surrogate munitions.

15. SUBJECT TERMS
Munitions, Mobility, Waves, Currents, Sediment Transport, Infragravity Waves, Bedforms, Boundary Layer, Edge Waves, Bedload Transport, Storm Waves, Northern Gulf of Mexico, UXO, Suspended Sediment

16. SECURITY CLASSIFICATION OF:			17. LIMITATION OF ABSTRACT	18. NUMBER OF PAGES	19a. NAME OF RESPONSIBLE PERSON
a. REPORT	b. ABSTRACT	c. THIS PAGE			Joseph Calantoni
UNCLASS	UNCLASS	UNCLASS	UNCLASS	48	19b. TELEPHONE NUMBER *(Include area code)* 228-688-4435

Table of Contents

List of Tables

List of Figures

List of Acronyms

ABS – Acoustic Backscatter
ADCP – Acoustic Doppler Current Profiler
ADV – Acoustic Doppler Velocimeter
AWAC – Acoustic Wave and Current Profiler
CT – Conductivity Temperature
FRF – Field Research Facility
FY – Fiscal Year
MR – Munitions Response
MRSON – Munitions Response Statement of Need
OBS – Optical Backscatter Sensor
ONR – Office of Naval Research
PC-ADP – Pulse Coherent Acoustic Doppler Profiler
PI – Primary Investigator
R/V – Research Vessel
SERDP – Strategic Environmental Research and Development Program
SSC – Suspended Sediment Concentration
TREX13 – Target and Reverberation Experiment 2013
UXO – Unexploded Ordnance

Keywords

Munitions
Mobility
Waves
Currents
Sediment Transport
Infragravity Waves
Bedforms
Boundary Layer
Edge Waves
Bedload Transport
Storm Waves
Northern Gulf of Mexico
UXO
Suspended Sediment

Acknowledgements

First we would like to thank our dedicated field team for all their support during the planning, deployment, maintenance, and retrieval operations. Conrad Kennedy was the lead technician for the fabrication of the targets. Tim Kooney was the lead technician for mounting design and instrument layout. Ed Braithwaite was lead technician for the sonar electronics and programming. Uriah Gravios was responsible for PC-ADP, OBS, and ADV programming. We thank our dive team including Duncan Greer, Viktor Adams, Uriah Gravois, and Kevin Briggs. Diver cores were taken by Kevin Briggs. Kevin Briggs and Jan Watkins performed sediment analysis in the laboratory. Allison Penko provided sediment transport rate calculations. Rob Holman performed preliminary analysis of our pencil beam sonar data. Kai Eldredge processed and analyzed the sector scanning sonar data including the manual tracking of munitions mobility between adjacent images. Advanced signal processing of our sector scanning sonar images was performed by Christian de Moustier. We thank our colleagues at APL-UW including Todd Hefner, Kevin Williams, and Dajun Tang for facilitating our collaboration with TREX13 and graciously accommodating our ship time and dive boat needs. We would like to thank the Captain and the crew for both the R/V Smith and the Fintastic for their gracious professionalism. We thank Clint Iles for keeping us safe during the deployment and retrieval.

1. Objective

Our objective was to provide detailed time series measurements of the in situ boundary layer processes responsible for munitions mobility including transport, burial, and excavation. We performed the first of a proposed set of field experiments to characterize the environment in which munitions are found while simultaneously recording the location of munitions relative to the seafloor at high spatial and temporal frequency. Unlike previous investigations that have provided before and after snapshots of munitions mobility, our instrumentation is capable of providing high spatial and temporal resolution measurements of all the relevant boundary layer processes (e.g., wave height and direction, current profiles, suspended sediment concentration, and sediment erosion and deposition) while simultaneously monitoring the mobility of surrogate munitions.

Our project was formulated in direct response to the Statement of Need for the Munitions Response Program Area (MRSON-13-02), which called for topics that include (1) assessing and predicting the location of munitions relative to the seafloor, and (2) assessing the environment in which munitions are found. Furthermore, information obtained on munitions locations may be used to assess the utility of various underwater sensor and survey approaches. To this end, our year 1 field effort had an ancillary objective to provide long term monitoring of waves and currents including high resolution measurements of boundary layer processes in cooperation with SERDP funded efforts during the Target and Reverberation Experiment (TREX13) held off the coast of Panama City, FL in April-May 2013. We are sharing data and collaborating with SERDP funded efforts including FY12 new start projects (MR-2229) “Inversion of High Frequency Acoustic Data for Sediment Properties Needed for the Detection and Classification of UXOs”, (MR-2230) “Data and Processing Tools for Sonar Classification of Underwater UXO”, and (MR-2231) “Acoustic Response of Underwater Munitions Near a Sediment Interface: Measurement-Model Comparisons and Classification Schemes”.

We hypothesize that the likelihood of mobility is not equal for all munitions and may be primarily quantified as a function of two (or more) non-dimensional parameters. In the initial field experiment, we deployed a range of surrogate munitions to test this hypothesis. Ultimately, we expect to provide answers to some fundamental questions about the fate of munitions that should be important to site remediation and management such as:

- May we classify groups of munitions as having relatively high or low likelihood of mobility?
- Do there exist groups of munitions that are more likely to be detected after energetic flow conditions (e.g., storms generating large gradients in sediment transport)?
- Does there exist a simple function of munitions characteristics (e.g., bulk density and size) that may be used to estimate the likely location of munitions relative to the bottom (i.e., from proud to some finite depth of burial)?
- Do there exist groups of munitions that have a high likelihood to be permanently buried regardless of site characteristics and changing environmental conditions?

Additionally, our measurements will be used to provide a baseline data set that process based models for prediction of munitions mobility (e.g., Vortex Lattice UXO Mobility Model) may utilize for verification and validation.

The project is at a Go/No-Go decision point for the proposed field effort to take place during year 2 at the US Army Corps of Engineers Field Research Facility (FRF) in Duck, NC. The Go/No-Go decision criterion as stated in the project brief to the Scientific Advisory Board held on 24 October 2012 was to be "based on results from Year 1 experiment and feedback from ongoing modeling studies." Here we will present the most significant results from the Year 1 experiment. Crucially, we did observe and quantify the mobility of surrogate munitions (ranging from 20 mm to 155 mm in size) including under moderate storm conditions, which occurred during TREX13. Perhaps, more interestingly, we also observed the rapid burial of surrogate munitions during the latter half of a storm event. Data analysis and interpretation is still ongoing. Here we present a snapshot of our observations with discussion and preliminary conclusions. Finally, we plan to receive feedback from ongoing modeling studies during an upcoming SERDP workshop to be coordinated by the Munitions Response Program.

2. Technical Approach

Our technical approach is to perform detailed field measurements of both munitions mobility and the simultaneous environmental conditions driving mobility for a range of surrogate munitions. Using sector scanning and pencil beam sonars we continuously monitored the mobility of munitions while simultaneously measuring time series data of the boundary layer hydrodynamics and sediment transport. Instruments were mounted on a pair of large rugged frames that were deployed at different water depths during TREX13. We are unaware of any existing data sets that include similar temporal resolution of munitions mobility coupled with detailed measurements of the relevant boundary layer dynamics in the natural environment.

The rest of Technical Approach will be broken into three subsections. The first subsection will describe the design and fabrication of the surrogate munitions used during TREX13. The second subsection will detail all of the instrumentation used in the study. The final subsection will describe the field experiment, including the deployment, maintenance, and retrieval of the instrumentation.

2.1. Surrogate Munitions

Guidance for the design and fabrication of surrogate munitions was limited. In the absence of access to inert certified munitions of the proposed type to be employed in our experiment, the following approach was used to design and fabricate surrogate munitions. We relied on crude drawings and specifications provided by existing Army Technical Manuals (e.g., TM 43-0001-27 and TM 43-0001-28) combined with low cost replicas that were purchased from Inert Products, LLC (http://www.inertproducts.com/). The purchased replicas were used to provide overall dimensions and shape details for the given munitions type. These purchased replicas were constructed from solid casts of urethane with varying density for the 155 mm and 81 mm and solid aluminum for the 25 mm and 20 mm (note the purchased 155 mm was positively buoyant and not deployed). Within the given overall dimensions of the purchased replicas, we then used computer aided design (CAD) tools to first develop mock munitions that would have approximately the known weights of explosive and overall weights provided by the Army Technical Manuals referenced above. The CAD versions of the mock munitions were used to provide moment of inertia estimates for the rolling moment about the long symmetry axis of the munitions. The estimated rolling moment of inertia, the overall weight, and the outer dimensions

were then used as the key features to design a set of surrogate munitions that could be readily fabricated from simple raw materials such as stainless steel, aluminum, and Delrin plastic. In all cases the rolling moment of inertia for our surrogate munitions were within 10% of the estimated rolling moment of inertia of the mock munitions as described above. In addition, the overall sizes and shapes nearly identically matched the overall sizes and shapes provided by the replica munitions from Inert Products, LLC. Likewise, the overall weights of the fabricated surrogate munitions were within 10-15% of the overall weights provided by the Army Technical Manuals.

We only used the rolling moment of inertia, the overall weight, and the outer dimensions in the design criterion for our surrogate munitions since our project is focused on munitions mobility. Our surrogate munitions will have a stark difference in their acoustic and electromagnetic response when compared to their real counterparts; however, we expect their mobility characteristics to closely resemble those of their real counterparts. It should be noted that a larger portion of this project than originally anticipated was expended on the design and fabrication of the surrogate munitions used during TREX13.

Additional replicas were fabricated from different materials with the same overall shape of the surrogate munitions to provide similar targets with different weights and rolling moments. These replicas were fabricated typically from a single solid material (e.g., stainless steel, aluminum, and Delrin plastic). We hypothesize that scaling laws developed for granular dynamics will be adaptable for a relevant range of munitions mobility conditions. The additional replica munitions constructed from solid materials with different densities were employed to aid in the testing of this hypothesis. Four different types of munitions were fabricated to be used in the experiments. A total of 4 surrogate munitions and 9 replicas were deployed around each of the two instrumentation frames. The complete list of deployed/recovered targets along with brief descriptions and their material properties is given in Table 1. The mass for each target was determined post fabrication prior to deployment. The density listed for the replicas fabricated from a single solid material is the known material density. The volume and rolling moments for all targets were estimated using CAD software. For the surrogates and replicas that are composites of more than one material the bulk density was estimated by combing the measured mass and the volume estimate from the CAD software.

The first and largest of the surrogate munitions fabricated for this project was modeled after the projectile, 155 mm, HE, M107, which was fired from 155 mm howitzers. Shown in Figure 1 is the CAD drawing for the mock (top) and the fabricated surrogate (bottom). Shown in Figure 2 is a photo of the fabricated surrogate, the purchased replica, and the replica fabricated from a single solid piece of aluminum from top to bottom, respectively.

The second of the surrogate munitions fabricated for this project was the 81 mm mortar. Shown in Figure 3 is the CAD drawing cutaway for the mock (top) and the fabricated surrogate (bottom). Shown in Figure 4 is a photo of the fabricated surrogate, the purchased replica, and the replica fabricated with a solid stainless steel body and aluminum tail section from top to bottom, respectively. The difference in rolling moment calculated for the 81 mm surrogate with and without fins is only 4.4%. While the fins seemingly add little to the total rolling moment, their interaction with the seafloor and bottom currents should not be underestimated.

Type	Labels	Materials	Source	Type	Recovered	Volume (in^3)	Mass (lb)*	Bulk Density ($lb\ in^{-3}$)	Rolling Moment ($lb\ in^2$)
155 mm, HE, M107	D5, D6	Delrin, 304 Stainless	Fabricated	Surrogate	D5, D6	468.9	75.3	0.161	316.3
	D3, D4	Aluminum	Fabricated	Replica	D3, D4	468.9	46.1	0.098	171.4
81 mm mortar	C3, C4	Delrin, 316 Stainless, Aluminum tail fins	Fabricated	Surrogate	C3, C4	73.8	8.3	0.112	8.471
	C5, C6	304 Stainless, Aluminum tail fins	Fabricated	Replica	C5, C6	73.8	19.2	0.260	17.30
	C1, C2	Urethane	Purchased	Replica	- , -	73.8	3.2	0.045	2.857
25 mm cartridge	B5, B6	Delrin, 316 Stainless	Fabricated	Surrogate	B5, B6	10.1	0.86	0.085	0.158
	B7, B8	304 Stainless	Fabricated	Replica	B7, B8	10.1	2.92	0.284	0.680
	B3, B4	Aluminum	Purchased	Replica	B3, B4	10.1	0.97	0.098	0.235
	B1, B2	Delrin	Fabricated	Replica	- , -	10.1	0.52	0.051	0.122
20 mm cartridge	A5, A6	Delrin, 316 Stainless	Fabricated	Surrogate	- , A6	4.7	0.45	0.096	0.046
	A7, A8	304 Stainless	Fabricated	Replica	A7, -	4.7	1.40	0.284	0.182
	A3, A4	Aluminum	Purchased	Replica	A3, A4	4.7	0.44	0.098	0.063
	A1, A2	Delrin	Fabricated	Replica	- , -	4.7	0.25	0.051	0.033

Table 1. *List of surrogate targets used during TREX13. A total of 26 targets were deployed and 18 targets were recovered. The mass (lb)* for each target was determined post fabrication.*

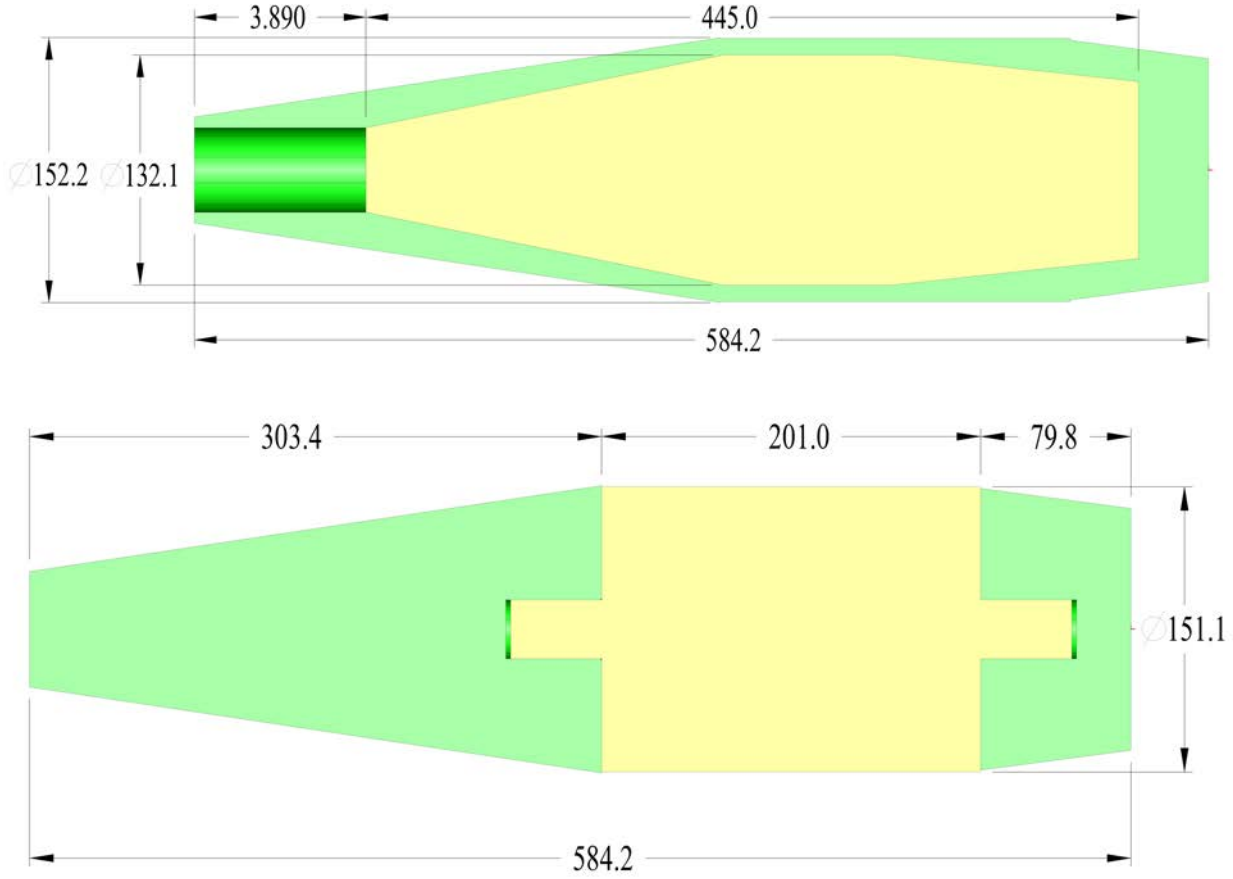

Figure 1. *(top) Shown is the mock design for the 155 mm, HE, M107 used for the inertia calculation. Here the yellow depicts material with the density of Comp B (15.4 lbs.) and the light green is assigned the density of steel. The dark green represents the fuze. (bottom) Shown is the fabrication design for the 155 mm, HE, M107 surrogate that we deployed in our experiment. Here the yellow depicts a solid stainless steel section and the light green ends depict solid Delrin plastic. All dimensions shown are in millimeters.*

Figure 2. *Photo of the surrogate (top), purchased replica (middle), and the replica fabricated from a single solid piece of aluminum (bottom) for the 155 mm, HE, M107 type. Note the purchased replica (middle) was determined to be positively buoyant and not deployed.*

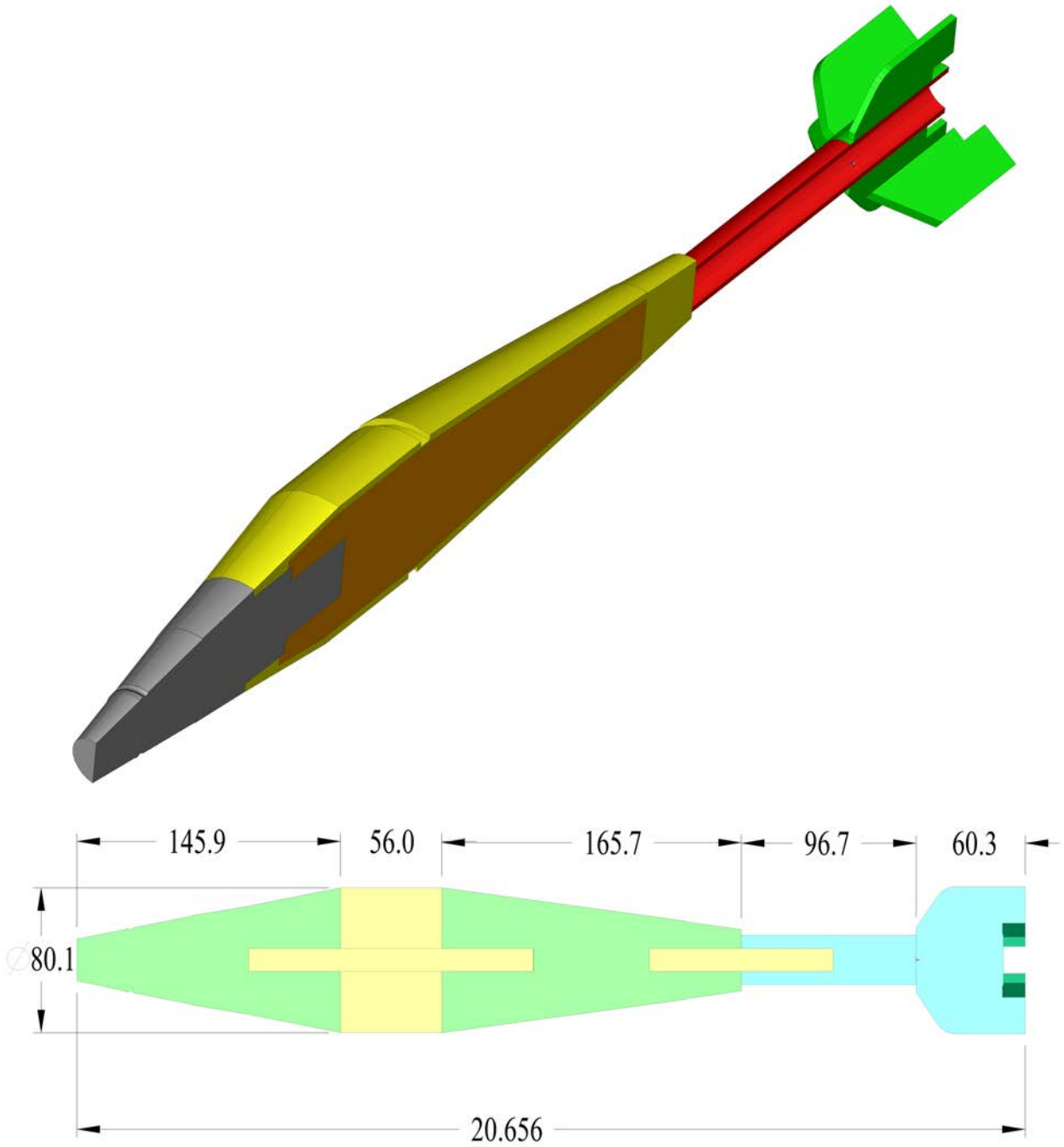

Figure 3. *(top) Shown is a cutaway image for the mock design for the 81 mm mortar used for the inertia calculation. Here the dark yellow depicts material with the density of Comp B (2.1 lbs.), the lighter yellow shell and red tail assembly were assigned the density of steel, the gray fuze was assigned the known weight (1.2 lbs.), and fins were assigned the density of aluminum. (bottom) Shown is the fabrication design for the 81 mm mortar surrogate that we deployed in our experiment. Here the yellow depicts a solid stainless steel section, the light green ends depict solid Delrin plastic, and the light blue tail assembly was constructed from solid aluminum. All dimensions shown are in millimeters.*

Figure 4. *Photo of the surrogate (top), purchased replica (middle), and the replica fabricated with a solid stainless steel body and aluminum tail section (bottom) for the 81 mm mortar type.*

The third and fourth of the surrogate munitions fabricated for this project were the cartridges, 25 mm and 20 mm. Shown in Figure 5 is the CAD drawing for the fabricated 25 mm (top) and the fabricated 20 mm (bottom). We did not create a mock CAD drawing these two types. The steel projectile was fabricated with nearly identical density and dimensions to those found in the Army Technical Manual. Fortuitously, in both cases, a solid piece of Delrin plastic cut in the shape of the shell casing very closely matches the weight of the remaining portion of the munitions. Note that while a steel projectile is very common for the 20 mm type, we realize that the projectiles for the 25 mm type may be much more sophisticated and varied. However, for the scope of this project we assumed the simplest solid steel projectile for the 25 mm type. Shown in Figure 6 are photos of the fabricated surrogate, the purchased replica, the replica fabricated with solid Delrin, and the replica fabricated with solid stainless steel from top to bottom, respectively.

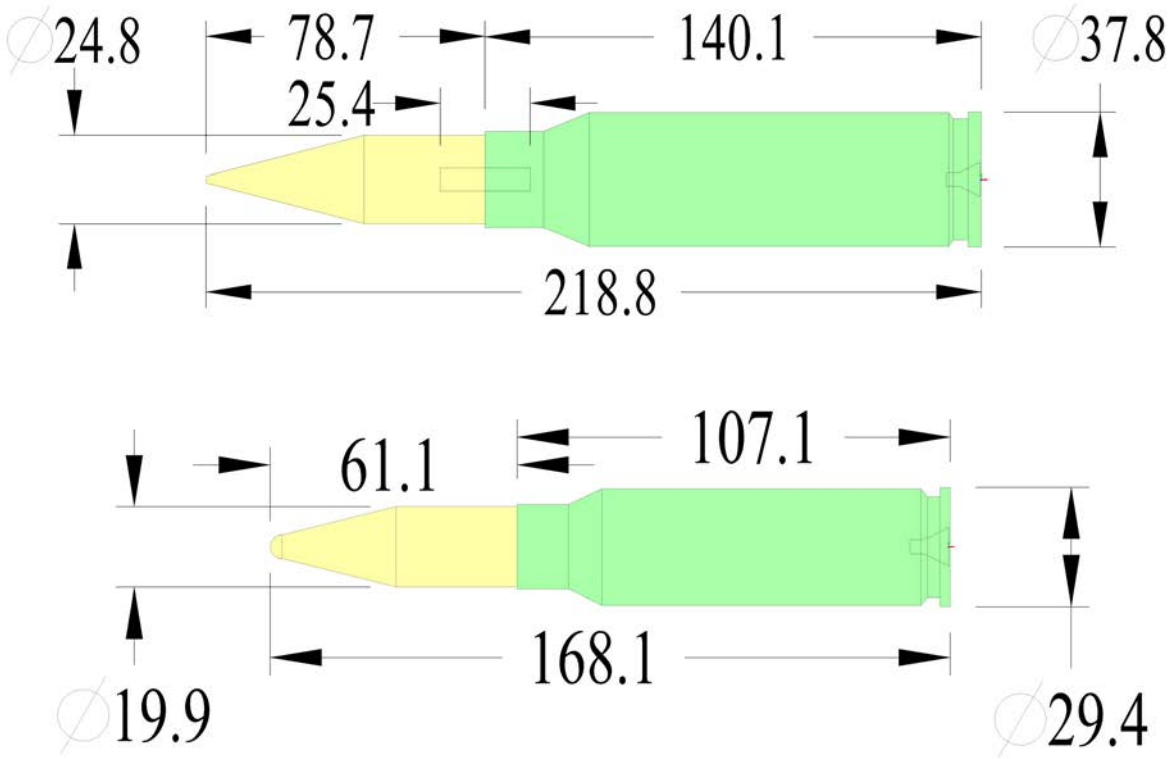

Figure 5. *Shown is the fabrication design for the 25 mm cartridge (top) and the 20 mm cartridge (bottom) that we deployed in our experiment. Here the yellow depicts a solid stainless steel projectile and the light green depicts solid Delrin plastic. All dimensions shown are in millimeters.*

Figure 6. *Photos of the surrogate (top), purchased replica (upper middle), the replica fabricated with solid Delrin (lower middle), and the replica fabricated with solid stainless steel (bottom) for the 25 mm cartridge type. Not shown was a similar set for the 20 mm type.*

2.2. Instrumentation

Instruments were mounted on a pair of large rugged frames (herein referred to as "quadpods") that were deployed at two different water depths (herein referred to as "deep" and "shallow") during TREX13. Sector scanning and pencil beam sonars were used to continuously monitor the mobility of munitions placed on the seafloor. A range of different acoustic Doppler current profilers (ADCPs) were used to measure the vertical profile of velocity at high spatial resolution near the bed and lower spatial resolution in the upper water column. Measurements of wave height and direction were obtained with an upward looking ADCP. Temperature, salinity, and pressure were also recorded near the bed. Optical sensors were paired with a pulse coherent acoustic Doppler profiler (PC-ADP) to provide downward looking measurements of the suspended sediment concentration in the wave bottom boundary layer. A comprehensive list of all the instrumentation deployed is found in Table 2.

Vendor/Type	Number	Frequency (kHz)	Temporal Resolution	Spatial Resolution	Recording Status	Purpose
Nortek AWAC	2	1,000	2 Hz for 20 minutes every half hour	50 cm bins from top of quadpod up to water surface	20 April – 23 May	Waves and currents
Nortek Aquadopp	4	2,000	2 Hz for 20 minutes every half hour	2.5 cm bins from top of quadpod down to seafloor	20 April – 23 May **(pair on shallow quadpod failed)	Currents and pressure
Imagenex 881	2	2,250	Once every 12 minutes	110 degree azimuth with 6 m range	20 April – 23 May	Target location and bed roughness
Imagenex 881A	2	600-1000	Once every 4 hours	180 degree azimuth and 60 degree polar with 2 m range	20 April – 23 May	Target location and bed elevation
Sontek PC-ADP	2	1,500	2 Hz continuous	5 cm bins from the seafloor up to 80 cm	20 April – 13 May (battery failure)	SSC, currents and pressure
OBS-3	4	N/A	2 Hz continuous	Single fixed location	20 April – 13 May (battery failure)	SSC
OBS-5	2	N/A	2 Hz continuous	Single fixed location	20 April – 23 May	SSC
SeaBird MicroCat	2	N/A	2 Hz continuous	Single fixed location	20 April – 13 May (battery failure)	Salinity and temp.
Sontek ADV*	2	10,000	100 Hz for 1 minute every half hour	Single fixed location	20 April – 23 May	SSC and turbulence

Table 2. *List of instrumentation deployed during TREX13. The number mounted on each quadpod is half the number given here *(Sontek ADVs only found on shallow quadpod).*

Recording intervals in both space and time were chosen within the constraints of the instrument capabilities to maximize use of available memory storage and estimated battery life. The only instrument failures were the two Nortek Aquadopps mounted on the shallow quadpod, neither of which recorded any data. The instruments have been operating normally on the bench and a failure point from the experiment still has not been identified. In practice, choices need to be made without a priori knowledge of how the instrument will respond at the field site of interest when programming the instrumentation. Gain levels and other settings are fixed based on best practices and estimates for the expected field site conditions. In most cases our choices for instrument settings were appropriate; however, there were some exceptions where intermittent portions of data records needed to be discarded because of saturated signals or other errors.

2.3. Field Experiment

The TREX13 field site in the northern Gulf of Mexico represents a typically lower energetic environment than other optional field sites on the east and west coast of the U.S. However, we do expect the results from the chosen field site to be readily applicable to other sandy field sites of both higher and lower average wave energy. Where the results and conclusions from this study may not be applicable will be at sites with substantially different sediment characteristics. For example, the results from our proposed sandy field site are very unlikely to have much value a few hundred miles to the west in the muddy Atchafalaya Bay, LA. For our purposes, TREX13 represented an experiment of opportunity where we were able to leverage resources and share data with other SERDP and ONR funded investigators.

We chose a simple two point, cross-shore transect for the locations of our two quadpods (Figure 7). After consultation with other TREX13 funded investigators we decided on the location for the deep quadpod to be ~1 km southwest from the center of the R/V Sharp moor box. The R/V Smith pulled up into a 2-point anchor and we deployed the deep quadpod at 1240 local time in about 20 m water depth (Figure 8). The GPS coordinates of the stern were logged as 30° 03.02330 N, 85° 41.33630 W, and the quadpod was marked with a small yellow float attached to a counter weight placed ~10 m to the east. Two dives (~20 minutes each) were performed to setup the deep quadpod and lay targets. Targets were laid on the seafloor around each quadpod according to a predetermined schematic shown in Figure 9. From the deep quadpod the R/V Smith plotted a course directly towards the shoreline. Again, the R/V Smith pulled up into a 2-point anchor and we deployed the shallow quadpod at 1600 local time in about 7.5 m water depth. The GPS coordinates of the stern were logged as 30° 04.80994 N, 85° 40.41064 W. No marker was attached. One dive operation (~30 minutes) was performed to setup the shallow quadpod and lay targets (Figure 10).

During the morning of 8 May 2013 maintenance dives were performed on each of the quadpods from the dive boat Fintastic. The timing of the maintenance dives had been delayed by about one week due to weather. Finally, on 23 May 2013, both quadpods were retrieved again using the R/V Smith. The diver observations recorded during the maintenance and retrieval dives will be presented below in the Results and Discussion Section. All instrumentation was recovered safely.

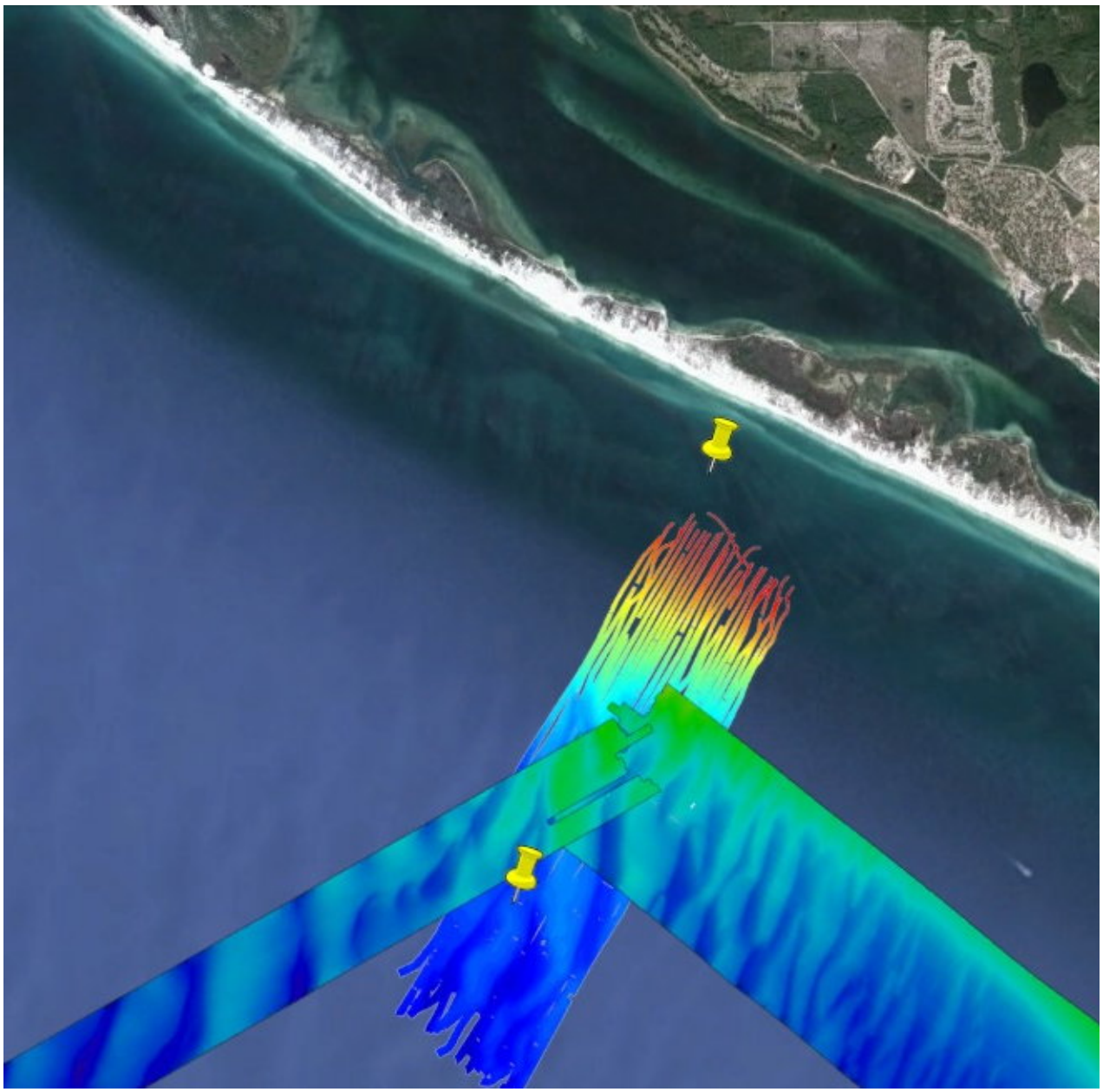

Figure 7. *Shown is a Google Earth © image for the field site off the coast of Panama City, FL. The yellow pins denote the locations of the shallow and deep quadpods, respectively. The underlying bathymetry swath oriented nominally shore normal extending from just offshore of the shallow quadpod out past the deep quadpod was surveyed during a pilot experiment in 2011. The other two overlaid swaths were surveyed during TREX13. Note the colormap is different for the two different surveys. (All bathymetry data provided by Christian de Moustier).*

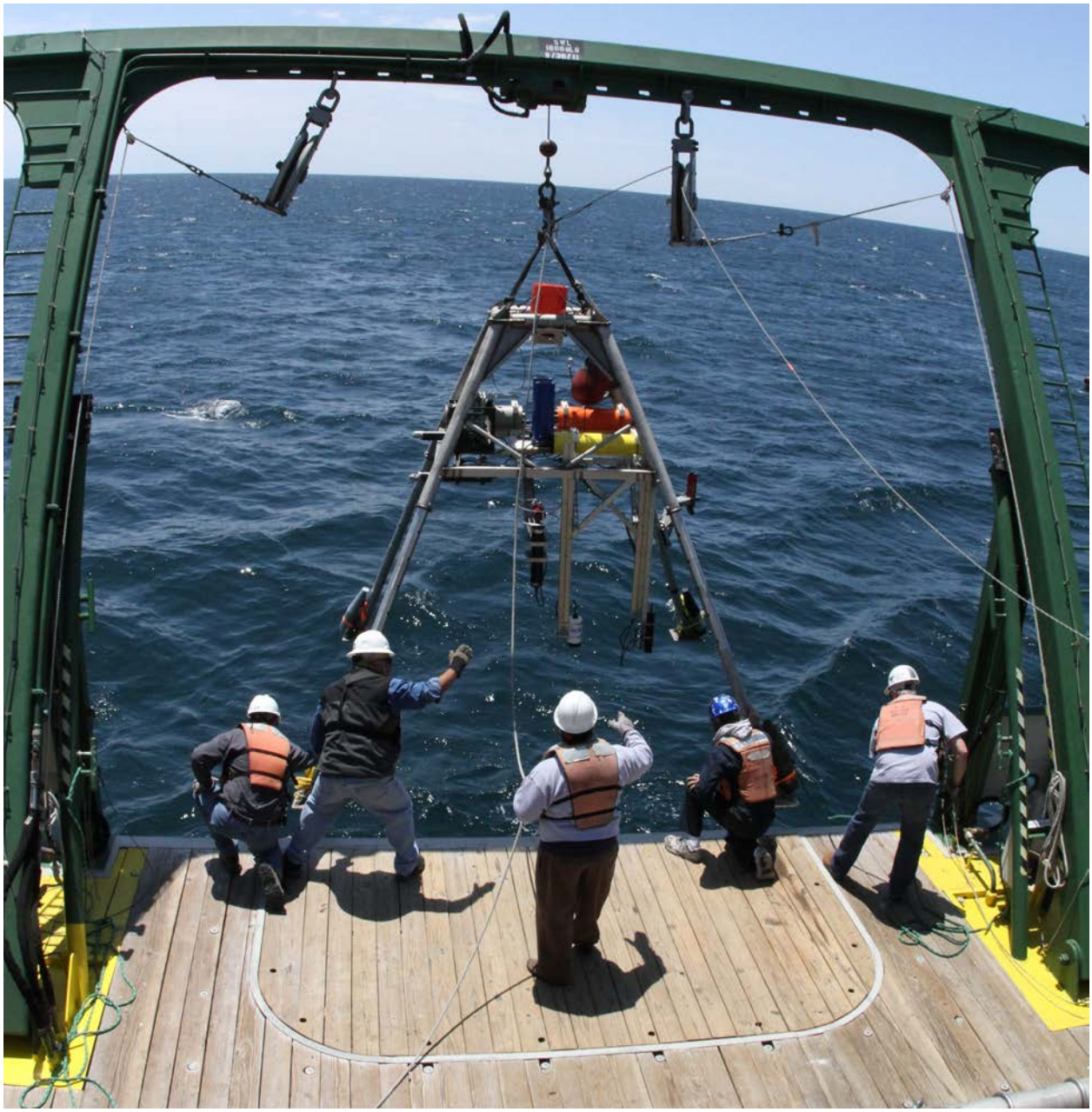

Figure 8. *Shown is a photo of the deep quadpod being deployed through the A-frame of the R/V Smith around 1240 local time on 20 April 2013. The deep quadpod was ~3.3 m tall and located in ~20 m depth.*

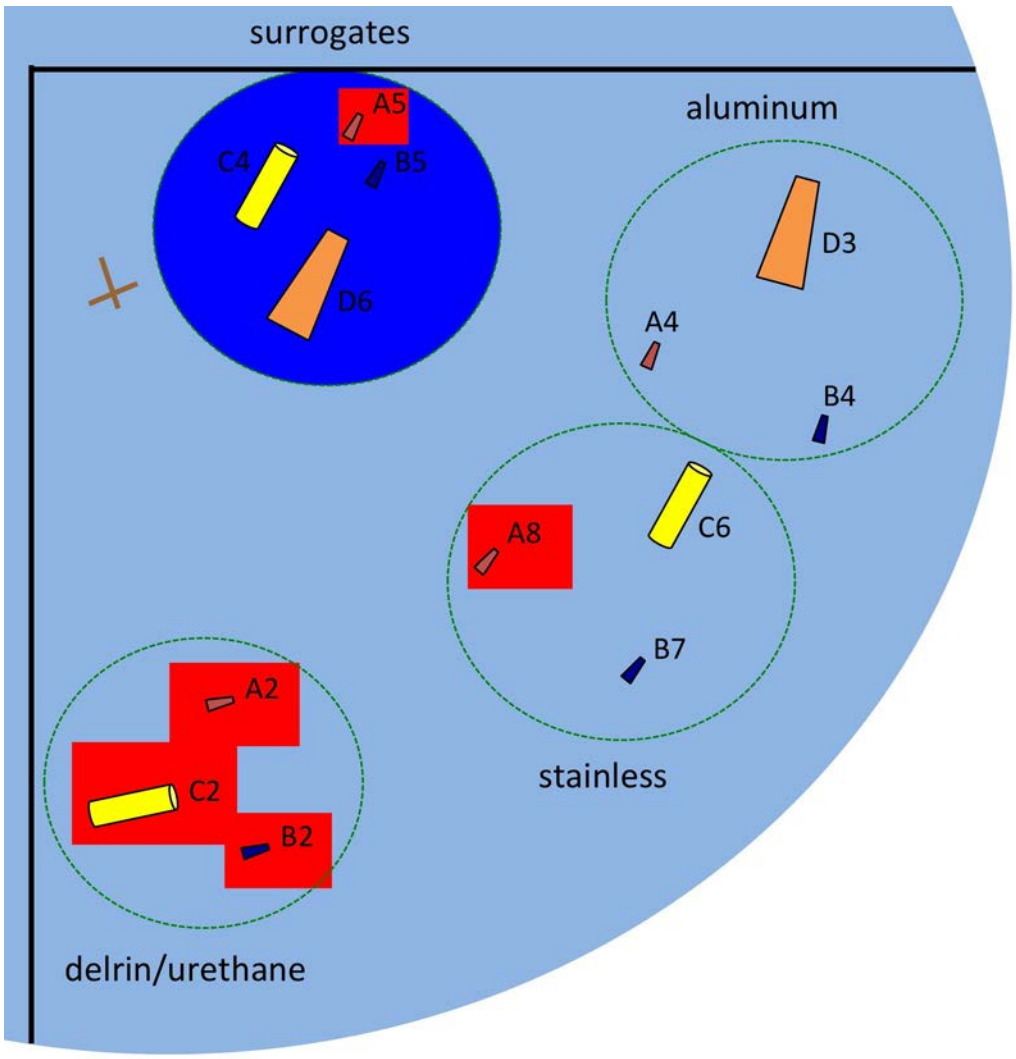

Figure 9. *Shown is the schematic used by divers to lay targets under the shallow quadpod. A similar layout was used under the deep quadpod. The light blue arc roughly denotes the field of view of the sector scanning sonar. The dark blue circle in the upper left denotes the field of view of the pencil beam sonar, which overlaps the sector scanning sonar field of view. Note the surrogates were placed in the overlap region as depicted above. The other replicas were grouped according to density. In this case the red boxes denote the targets that were not recovered from the shallow quadpod site.*

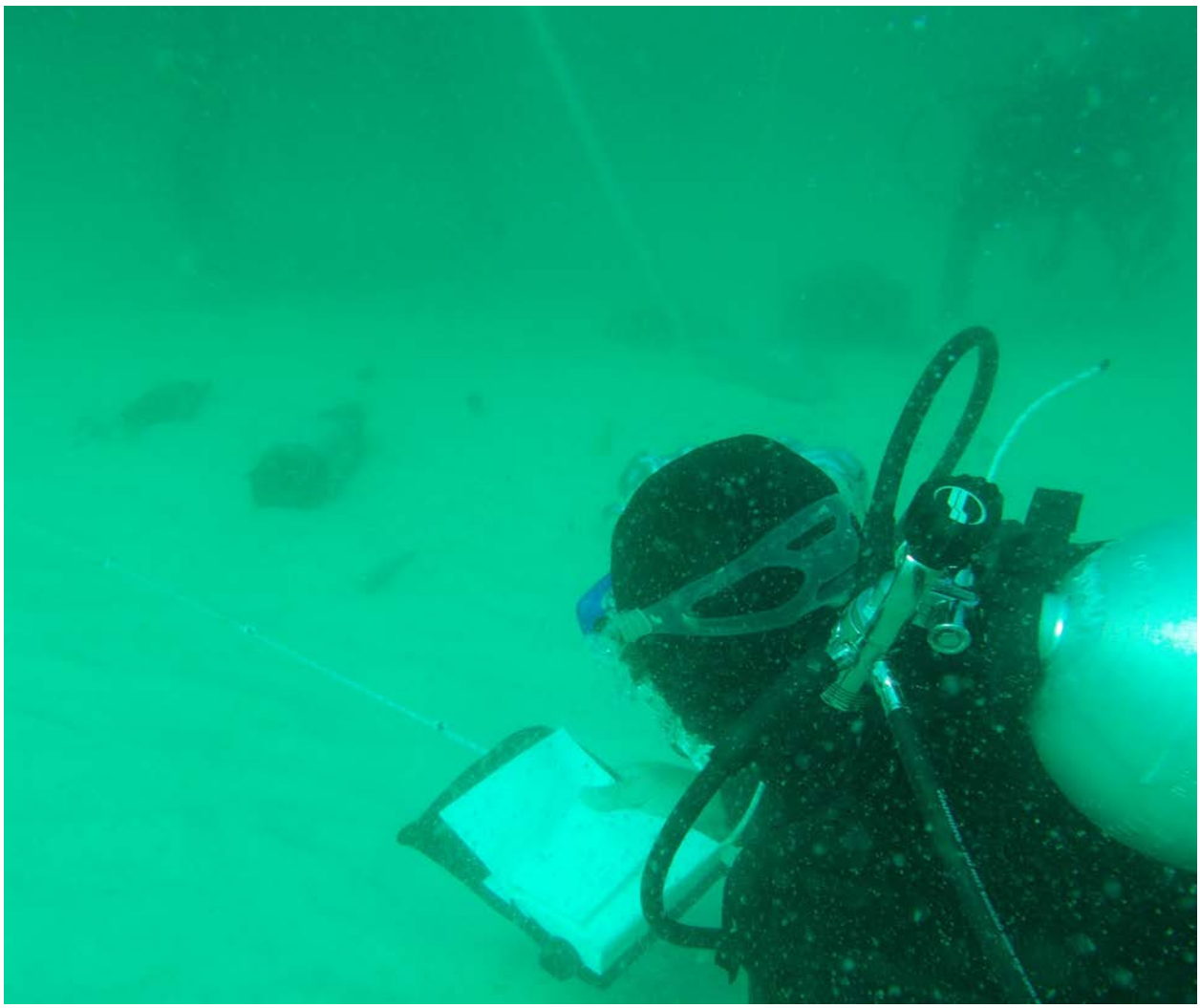

Figure 10. *Shown is a photo of divers laying the target field during the shallow quadpod deployment. One leg of the quadpod is visible in the upper center of the photo. The shallow quadpod was ~2.3 m tall and located in ~7.5 m depth.*

3. Results and Discussion

The Go/No-Go decision criterion as stated in the project brief to the Scientific Advisory Board held on 24 October 2012 was to be "based on results from Year 1 experiment and feedback from ongoing modeling studies." The first criterion is the results of the Year 1 field experiment presented here. The data shows that we observed the onset of munitions mobility for the largest munitions including the 155 mm surrogate. Perhaps even more interestingly, we observed the burial of the entire target field at the shallow quadpod location including the 155 mm surrogate immediately following the mobility event. The observed rapid and shallow burial of our target field at the shallow quadpod site provides a unique and challenging data set for ongoing modeling studies, particularly when coupled with the data sampled simultaneously at the deep quadpod location where limited mobility and no burial were observed. We believe we have sufficient data available that includes the munitions type along with the observed mobility,

detailed hydrodynamic conditions (across the water column), and sediment characteristics and transport conditions at high temporal frequency to provide ongoing modeling studies with a unique and challenging benchmark data set. To this end, we have satisfied the first criterion of the Go/No-Go decision. The second criterion to be based on feedback from modeling studies is yet to be completed. We plan to receive feedback from ongoing modeling studies during an upcoming SERDP workshop to be coordinated by the Munitions Response Program.

Munitions mobility and burial for the largest surrogates and replicas deployed was observed at the shallow quadpod location in ~7.5 m water depth during the passage of an atmospheric front, 5 – 6 May 2013. During the same storm event, similar munitions mobility and sediment transport was not observed at the deep quadpod location in ~20 m water depth. As anticipated based on the wave climatology available from NOAA buoy observations in the region over the past three years, we observed the onset of energetic conditions that mobilize munitions in shallow water. The more surprising observation was the subsequent and rapid burial of all surrogate and replica munitions during a 24-hour period following the mobility. A maintenance dive was performed on the morning of 8 May 2013 immediately after the storm event and found a single clue that the surrogates and replicas may have been buried in place as opposed to being transported away by the waves and currents (Figure 11). Divers were able to recover a total of 8 munitions buried in place at the shallow quadpod location during the maintenance dive performed on 8 May 2013 (Figure 9). Divers excavated munitions by hand based on the known initial locations in the target field; a metal detector was not available. Consequently, we believe that the unrecovered munitions, A5 and A8, also were buried in the target field but due to their small size were not found during hand excavation. The other unrecovered targets, A2, B2, and C2, were believed to have been transported away from the target field due to their low density and high mobility as expected. Similar replica munitions deployed at the deep quadpod location were also not recovered and no burial of any targets was observed at that location. Note the munitions excavated by the divers at the shallow quadpod location on 8 May 2013 were immediately redeployed for the duration of the experiment as shown in Figure 9.

An overview of the wave conditions including the significant wave height, direction, and frequency spectra are plotted (Figure 12) for the shallow (upper a,b) and deep (lower a,b) quadpod locations from the start of the experiment through 13 May. Note data exists through 23 May but conditions remained quiescent and uneventful between 13 and 23 May. The spectral shapes given in Figure 12b (upper and lower) were estimated as bottom pressure variance spectra (m^2) normalized by frequency peak variance. The faster variance decay with frequency seen at the deep site is due to the natural attenuation of high frequency energy with depth. A remarkable feature (both deep and shallow site) is the significant infragravity content (frequencies lower than 0.05 Hz). Due to the low frequency, these modes are only weakly attenuated with the water depth. We will discuss the potential significance of the low frequency energy later in the report.

An overview of the observed munitions mobility throughout the deployment is shown for both the shallow (Figure 13) and deep (Figure 14) quadpod locations. The target locations were determined from sector scanning sonar images. Based on the known initial locations during the deployment, we identified and plotted targets when their locations shifted or they were not visible between successive sector scanning sonar images. At both the shallow and deep quadpod locations the solid Delrin (A1, A2, B1, B2) and urethane (C1, C2) replicas were not recovered.

Due to their low density and consequently high mobility these targets all disappeared from the field of view of the sector scanning sonar images early during the experiment. All of the remaining targets except for A5 and A8 deployed at the shallow quadpod location were recovered.

The remainder of the Results and Discussion will focus on the mobility and burial that occurred at the shallow quadpod location during the storm event on 5-6 May. Note this event was responsible for the mobility and burial of the largest surrogate and replica munitions mentioned above (Figure 11). Elevation reported at each quadpod location will be given in meters with the origin set at the bottom of the quadpod positive upward. Tilt and pressure sensors indicated both quadpods remained in fixed positions for the duration of the deployment.

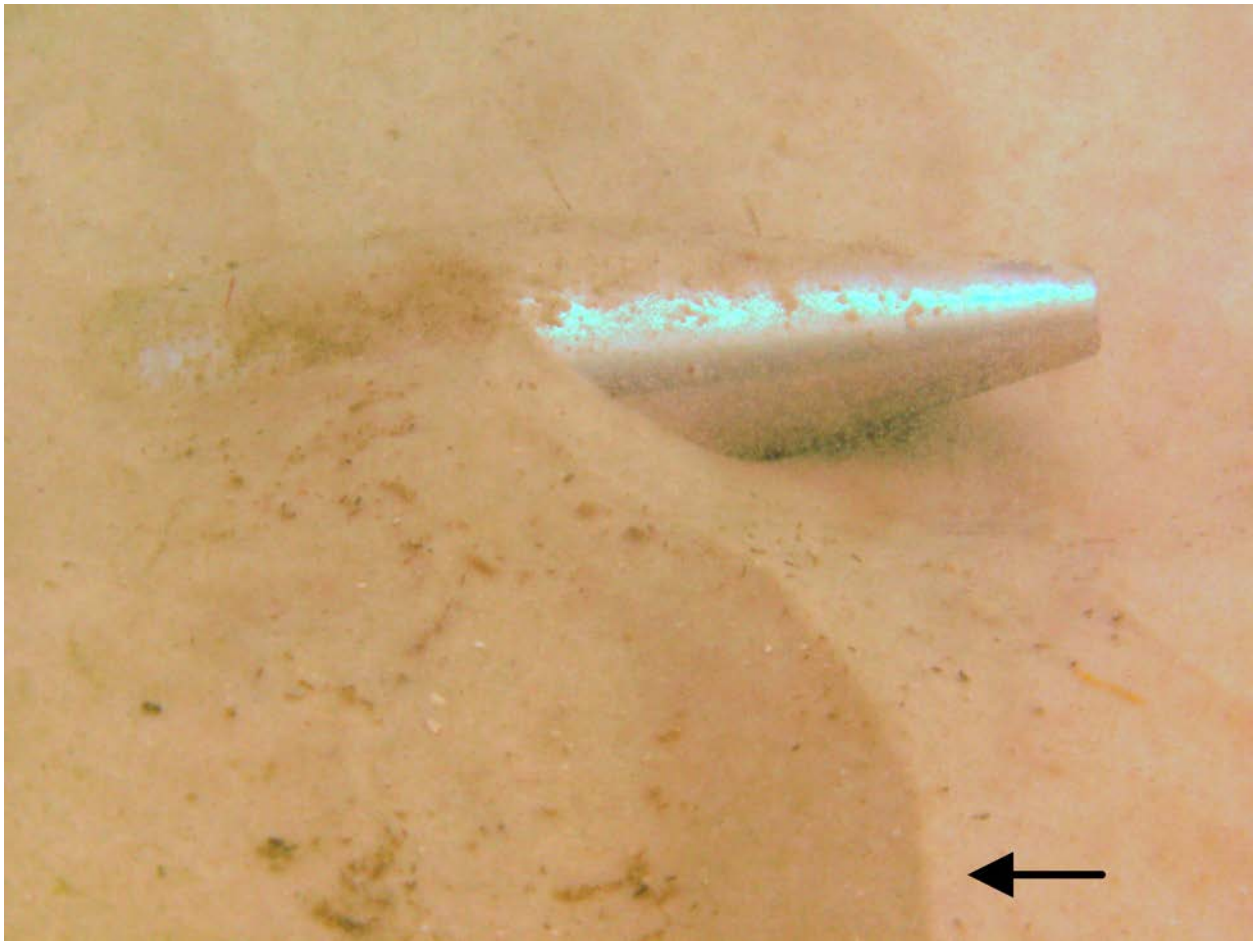

Figure 11. *Shown is a diver photo from the target field of the shallow quadpod taken on the morning of 8 May 2013. The 155 mm replica fabricated from solid aluminum was partially buried in the crest of a sand ripple. The sharp crest of the ripple (or bedform) is visible in the foreground of the image, indicated by the black arrow. The replica shown here was the only target not completely buried during the storm event at the shallow quadpod location.*

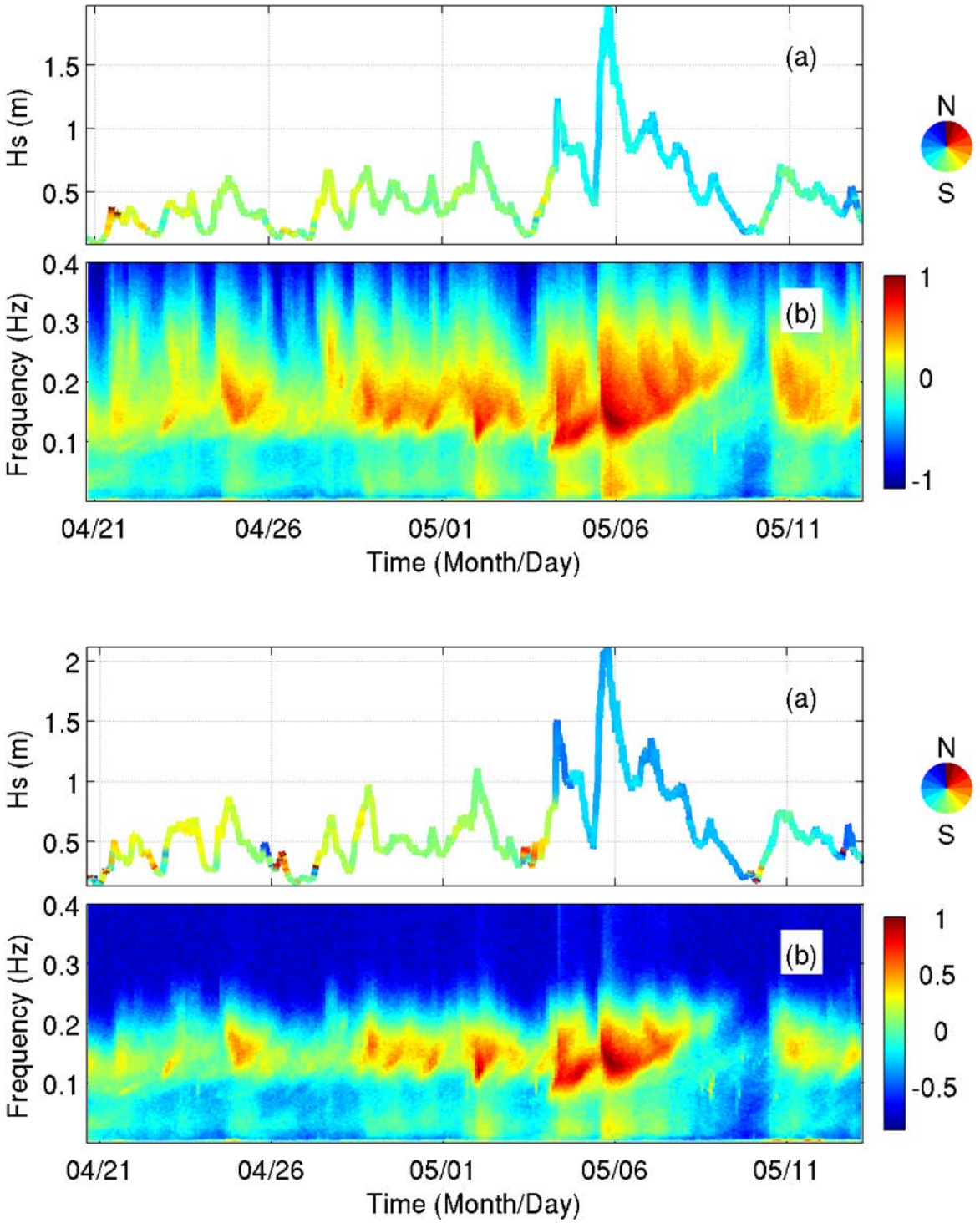

Figure 12. *Shown is the significant wave height and direction (a) and the normalized wave frequency spectrum (b) for the shallow (top) and deep (bottom) quadpod locations. The color of the line (panels a) denotes the propagating from direction of the waves.*

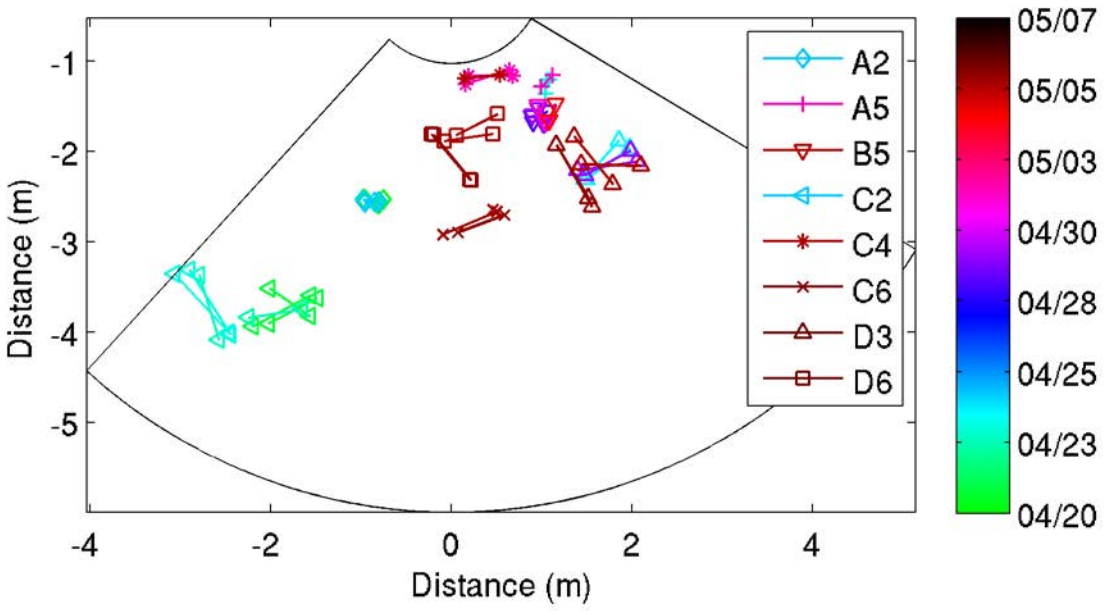

Figure 13. *Using sector scanning sonar images we tracked the positions for all visible targets at the shallow quadpod location up to the maintenance dive performed on 8 May. The color of the symbol in the legend denotes the last time when each target was visible. Targets A2 and C2 were immediately mobile and transported out of the field of view. Contact with target A5 was lost around 2 May. Targets B5, C4, C6, D3, and D6 were all buried during the storm event from 5-6 May and recovered during the maintenance dive on 8 May.*

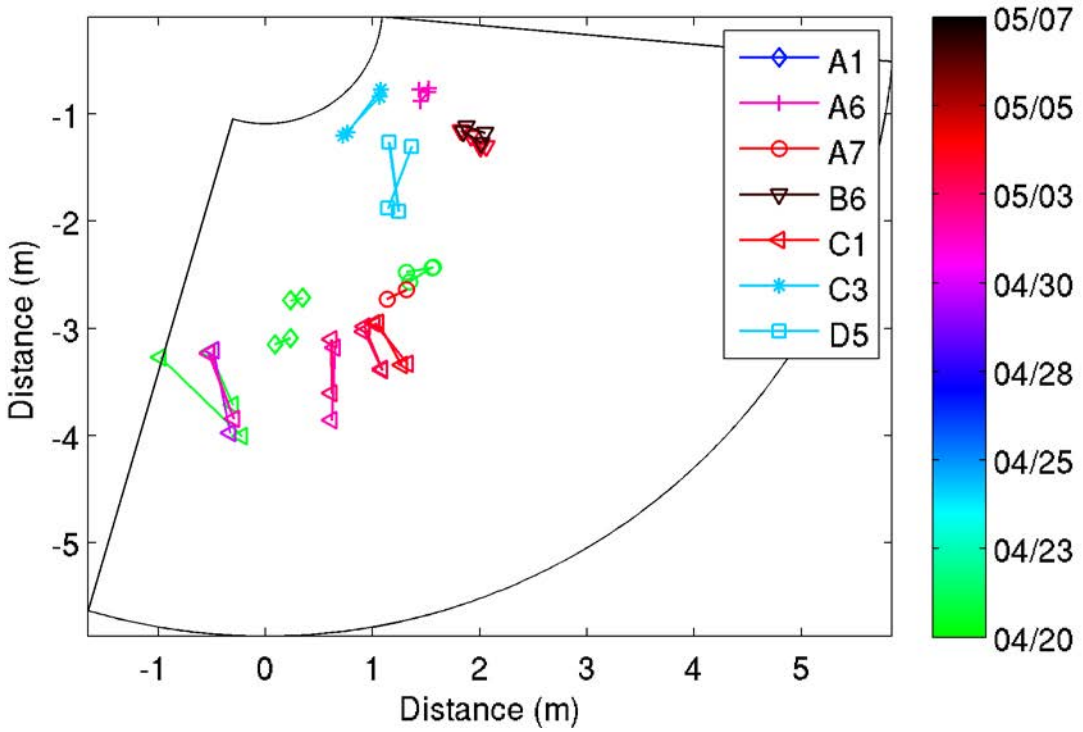

Figure 14. *Using sector scanning sonar images we tracked the positions for all visible targets at the deep quadpod location up to the maintenance dive performed on 8 May. The color of the symbol in the legend denotes the last time when each target was visible. Limited mobility of targets was observed. All targets were recovered at the deep quadpod location except for A1, B1, and C1, which were believed to have been transported away from the target field due to their low density and high mobility as expected.*

3.1. Storm Event

The storm event on 5-6 May was of particular interest. During the interval we observed large wave energy, munitions mobility (all densities and sizes) and changes in suspended sediment concentration and bed elevation. The event was characterized by significant wave heights in excess of 2 m with peak periods ~7 s at both quadpod locations. The wave directional spectra calculated at 1800 on 5 May during the peak of the event are shown for the shallow (Figure 15) and deep (Figure 16) quadpod locations. Mean currents measured in the upper water column at both shallow (Figure 17) and deep (Figure 18) quadpod locations are shown along with mean surface elevation denoted by the solid black line. For the majority of the event, mean currents in the water column were primarily moving towards the SE direction (or alongshore) at both quadpod locations with mean current magnitudes modulating with wave height at the deep quadpod location. Mean currents measured near the bed (initial bed level set at $z = 0$) at both the shallow (Figure 19) and deep (Figure 20) quadpod locations are shown. Mean currents near the bed at the shallow quadpod location are weak in magnitude; however, they will be discussed in more detail later. At the deep quadpod location, mean currents were maximized as the front approached during the morning of 5 May and decreased by mid-day. Data was excluded in Figure 19c as it becomes impossible to accurately estimate direction as the mean current

magnitude approaches zero. Additionally, contaminated data due to consecutive pulse interference in the PC-ADP was excluded in Figure 20.

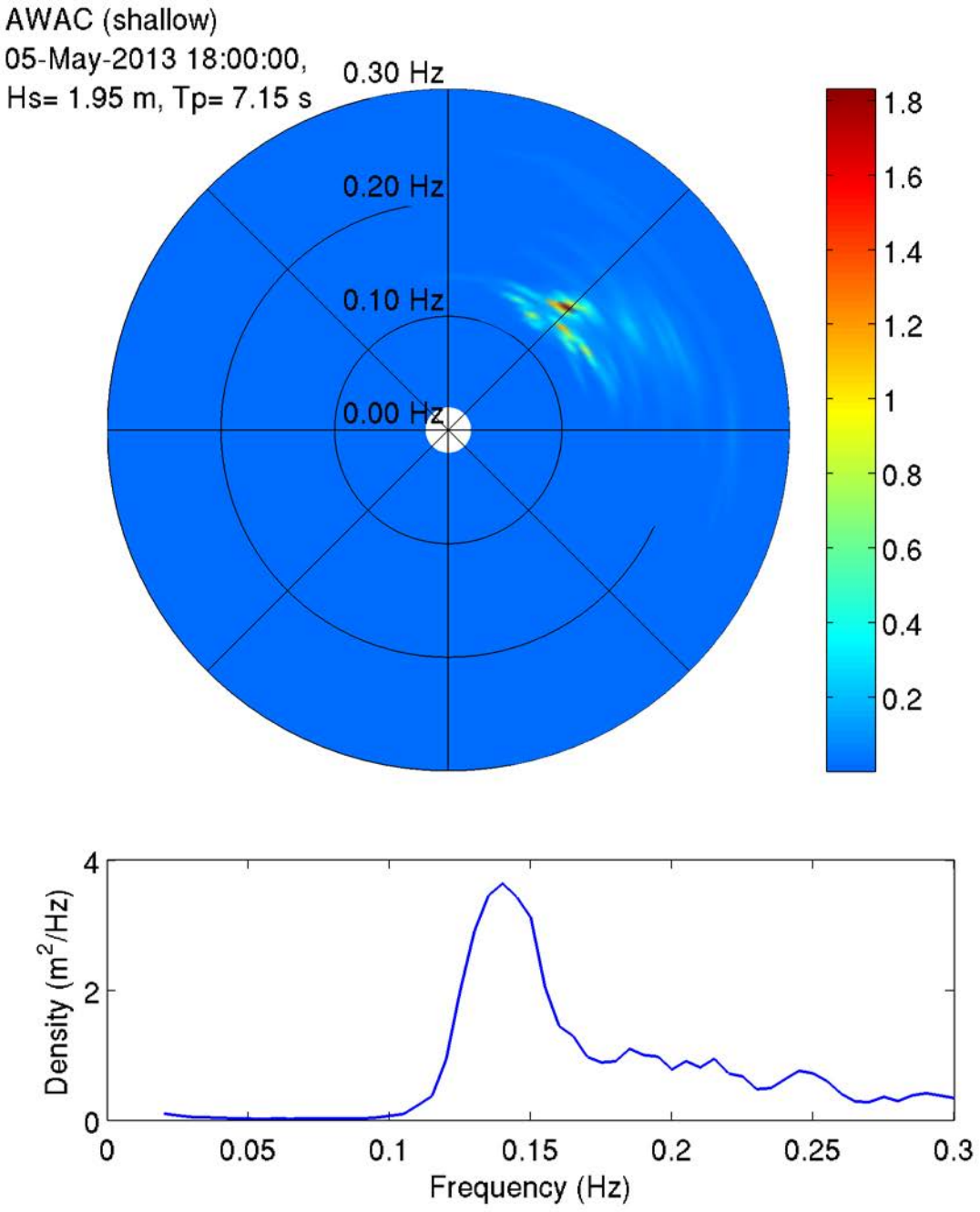

Figure 15. *Directional spectrum (top) and spectral density (bottom) (m^2/Hz) of free surface elevation measured at the shallow quadpod on 5 May at 1800.*

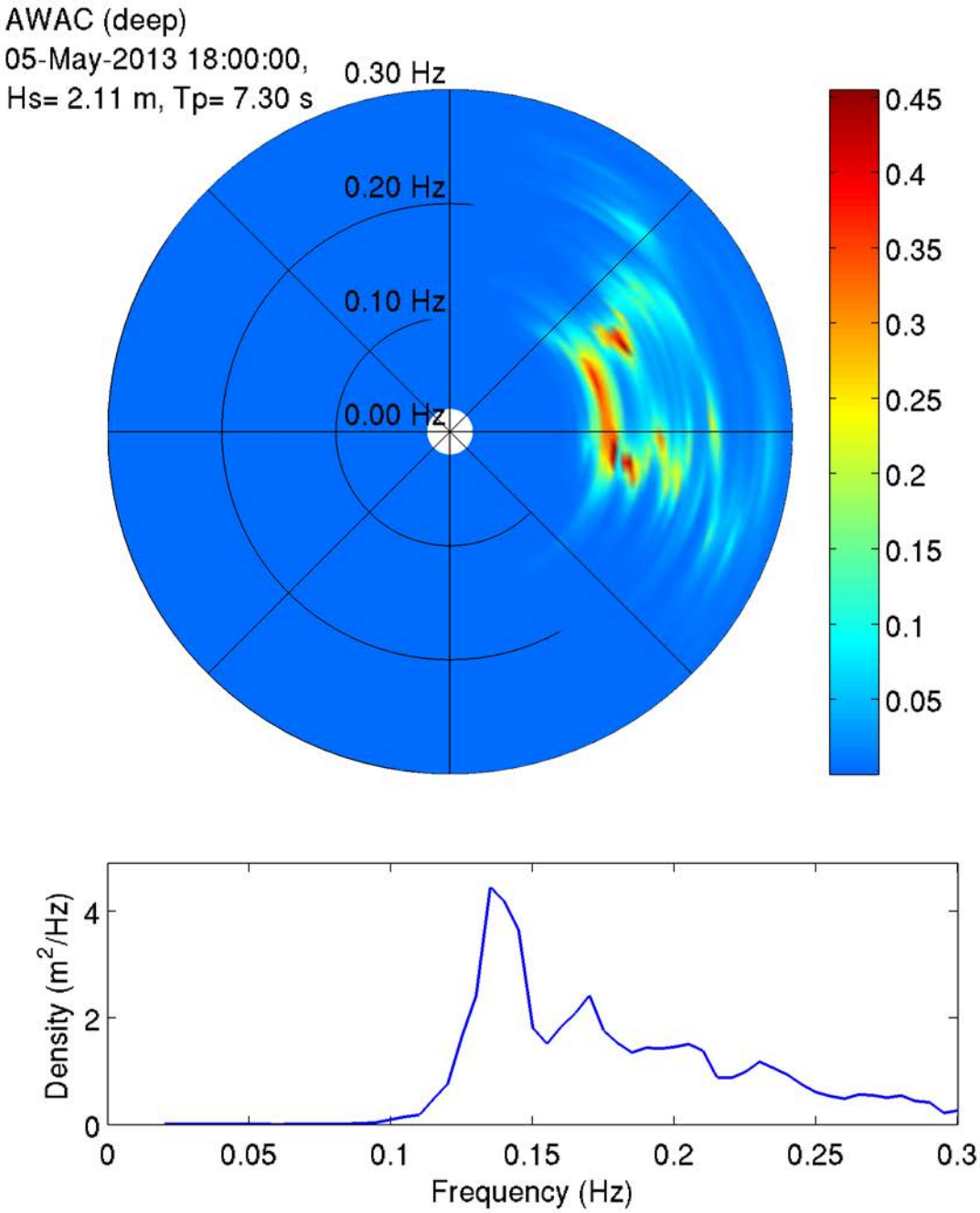

Figure 16. *Directional spectrum (top) and spectral density (bottom) (m^2/Hz) of free surface elevation measured at the deep quadpod on 5 May at 1800.*

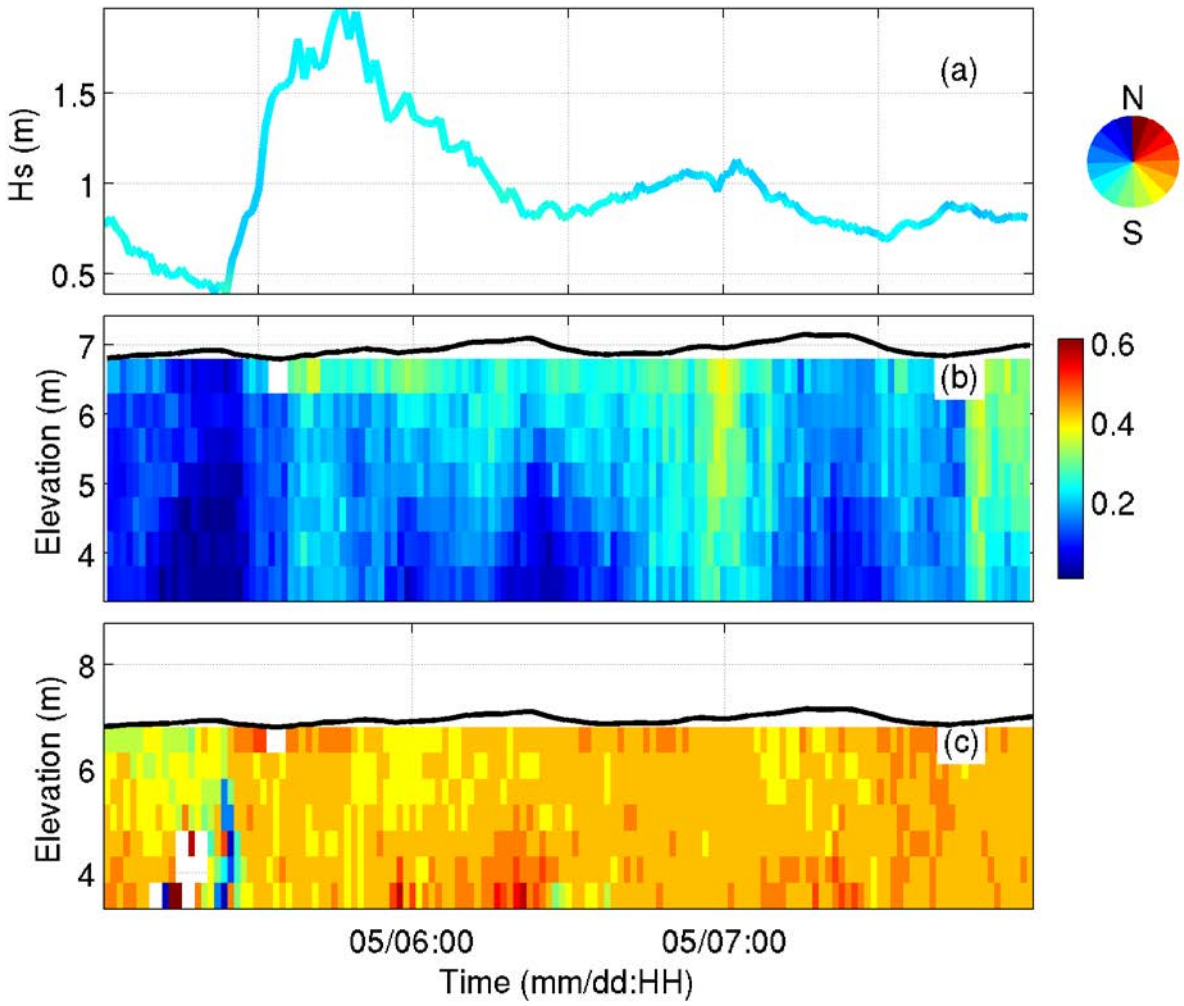

Figure 17. *Shown is significant wave height and direction (a) reported as coming from, mean current speed (m/s) and mean surface elevation (solid black line) (b), along with mean current direction (c) reported as flowing towards using same color wheel (a) at the shallow quadpod location.*

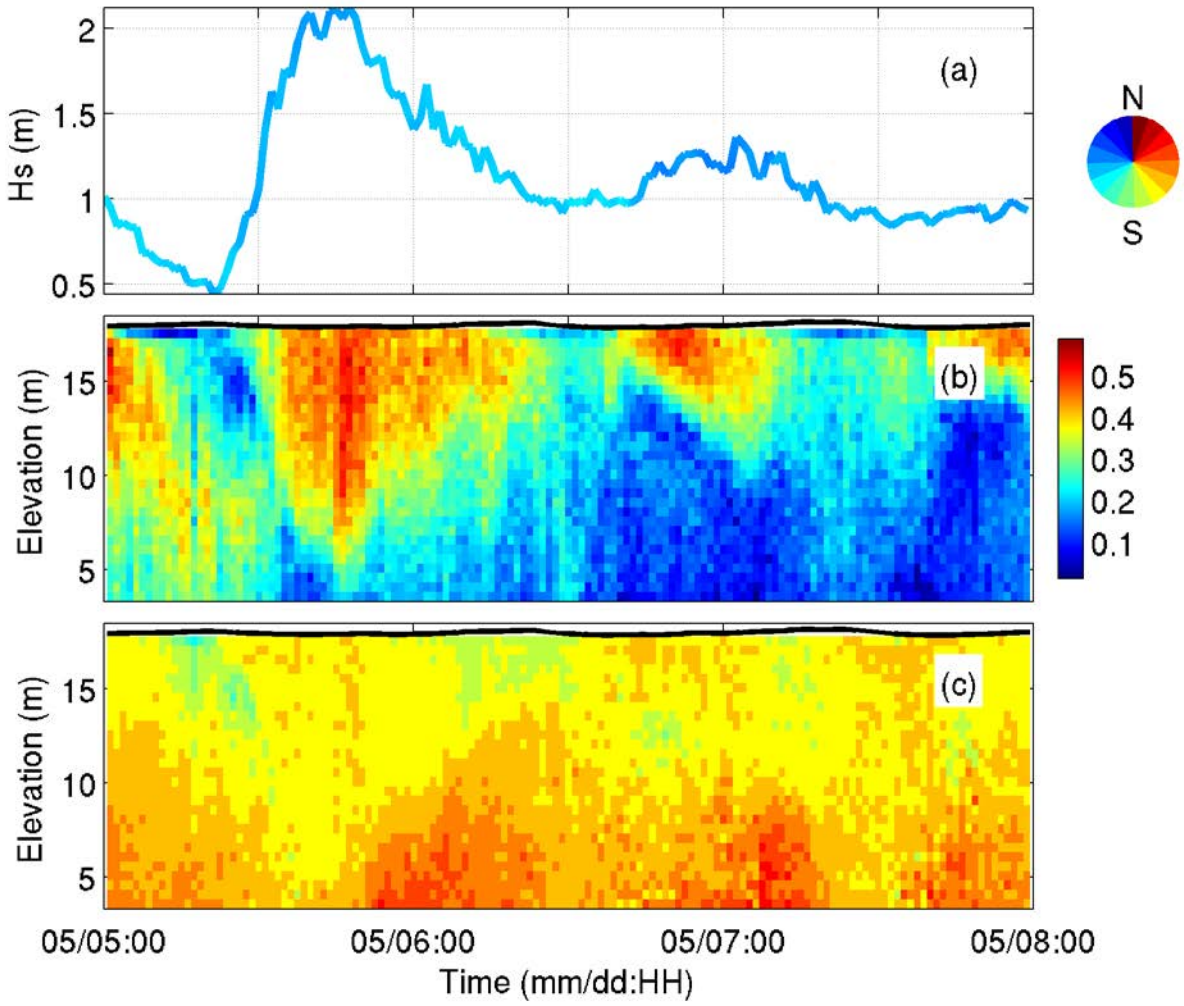

Figure 18. *Shown is significant wave height and direction (a) reported as coming from, mean current speed (m/s) and mean surface elevation (solid black line) (b), along with mean current direction (c) reported as flowing towards using same color wheel (a) at the deep quadpod location.*

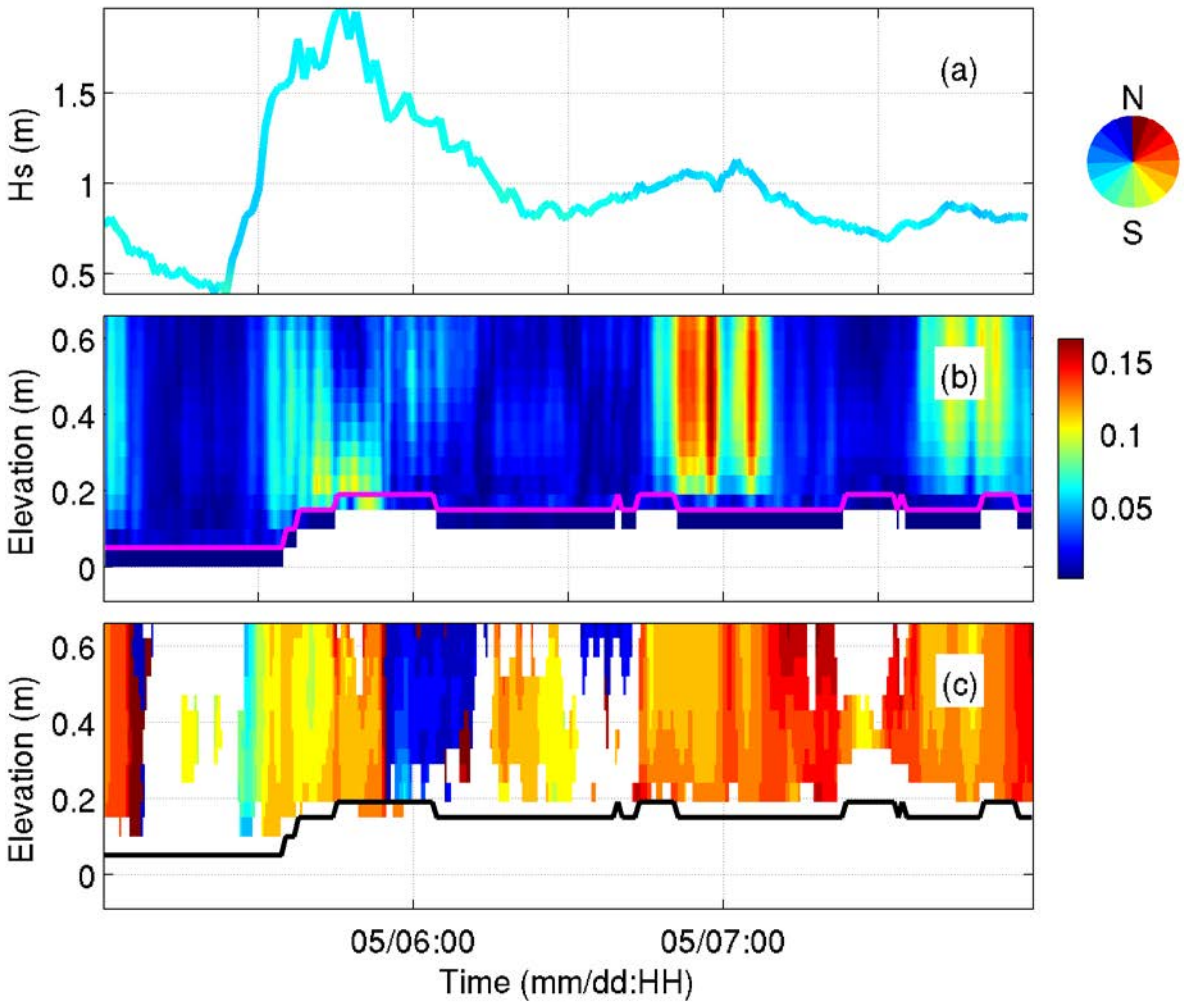

Figure 19. *Shown is significant wave height and direction (a) reported as coming from, mean current speed (m/s) and bed level estimated from maximum backscatter intensity (solid magenta line) (b), along with mean current direction (c) reported as flowing towards using the same color wheel (a) and bed level estimated from maximum backscatter intensity (solid black line) at the shallow quadpod location.*

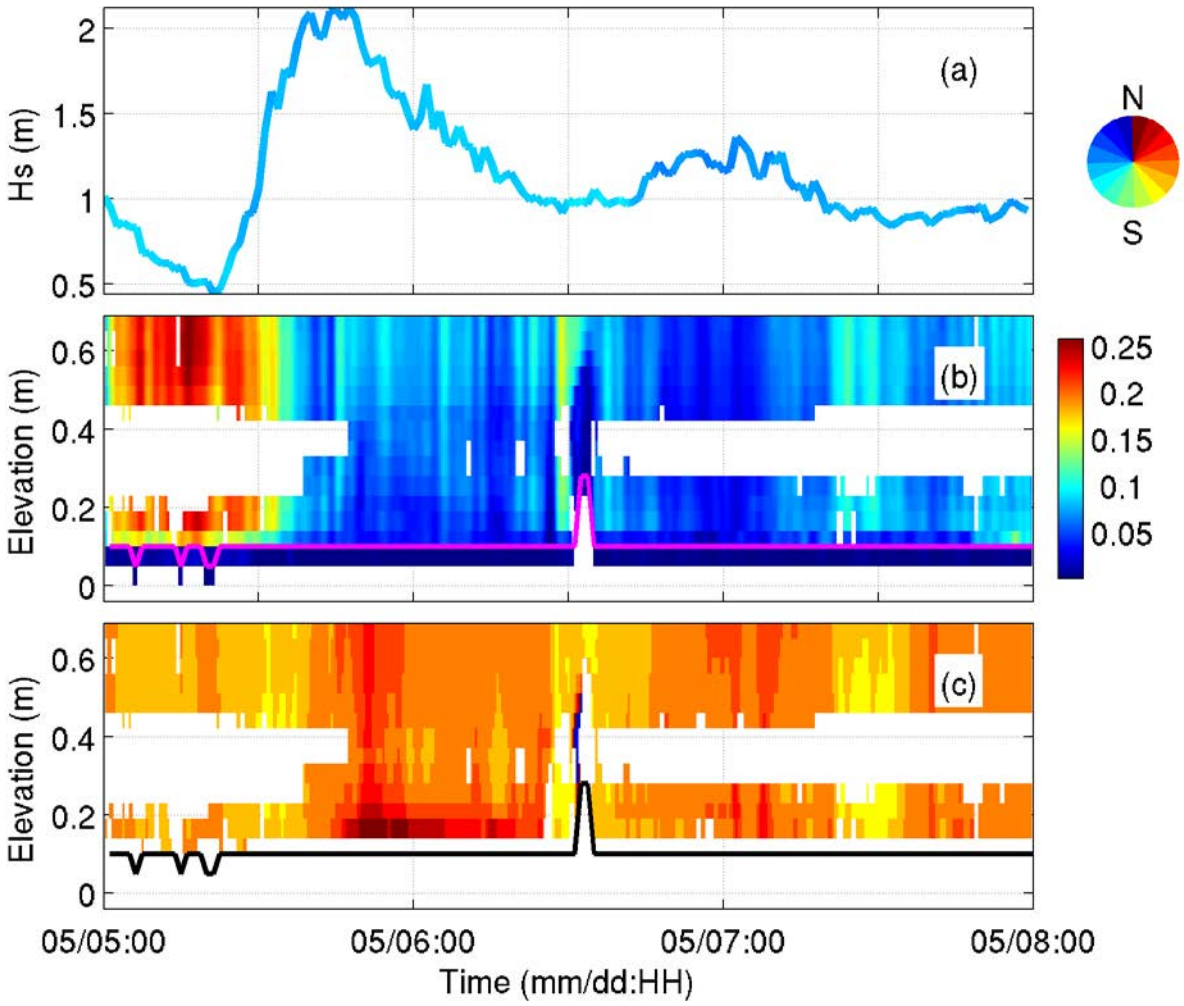

Figure 20. *Shown is significant wave height and direction (a) reported as coming from, mean current speed (m/s) and bed level estimated from maximum backscatter intensity (solid magenta line) (b), along with mean current direction (c) reported as flowing towards using the same color wheel (a) and bed level estimated from maximum backscatter intensity (solid black line) at the deep quadpod location.*

Suspended sediment concentrations observed near the bed are visually correlated to peak wave conditions for both the shallow (Figure 21) and deep (Figure 22) quadpod locations. Between 1600-2200 on 5 May, the location of the maximum acoustic backscatter (ABS) intensity, typically used to estimate the at rest bed elevation, shifted upward by 15 cm at the shallow quadpod location (Figure 21c). However, preliminary analysis of the pencil beam and sector scanning sonar data suggested that the bed level increase actually occurred throughout the first half of the day, 6 May. Although suspended sediment was observed near the bed at the deep quadpod location no changes in bed elevation were observed. The brief spike observed in ABS during the afternoon of 6 May (Figure 22c) may be due to biological activity (e.g., fish).

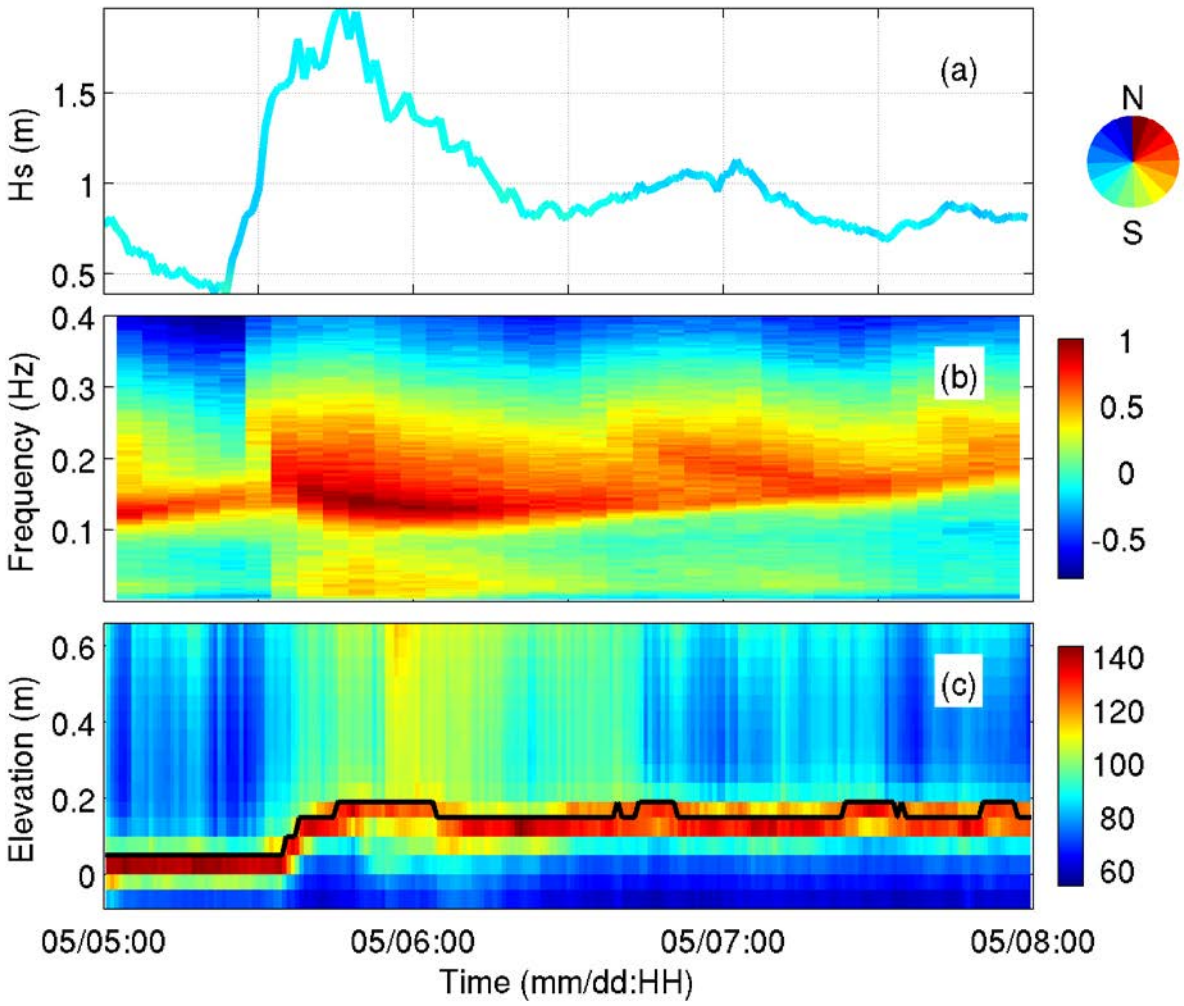

Figure 21. *Shown is significant wave height and direction (a) reported as coming from, mean b) free surface spectral density (b) estimated from pressure record, and acoustic backscatter intensity (counts) near the bed (c) with contour of maximum backscatter (solid black line) at the shallow quadpod location.*

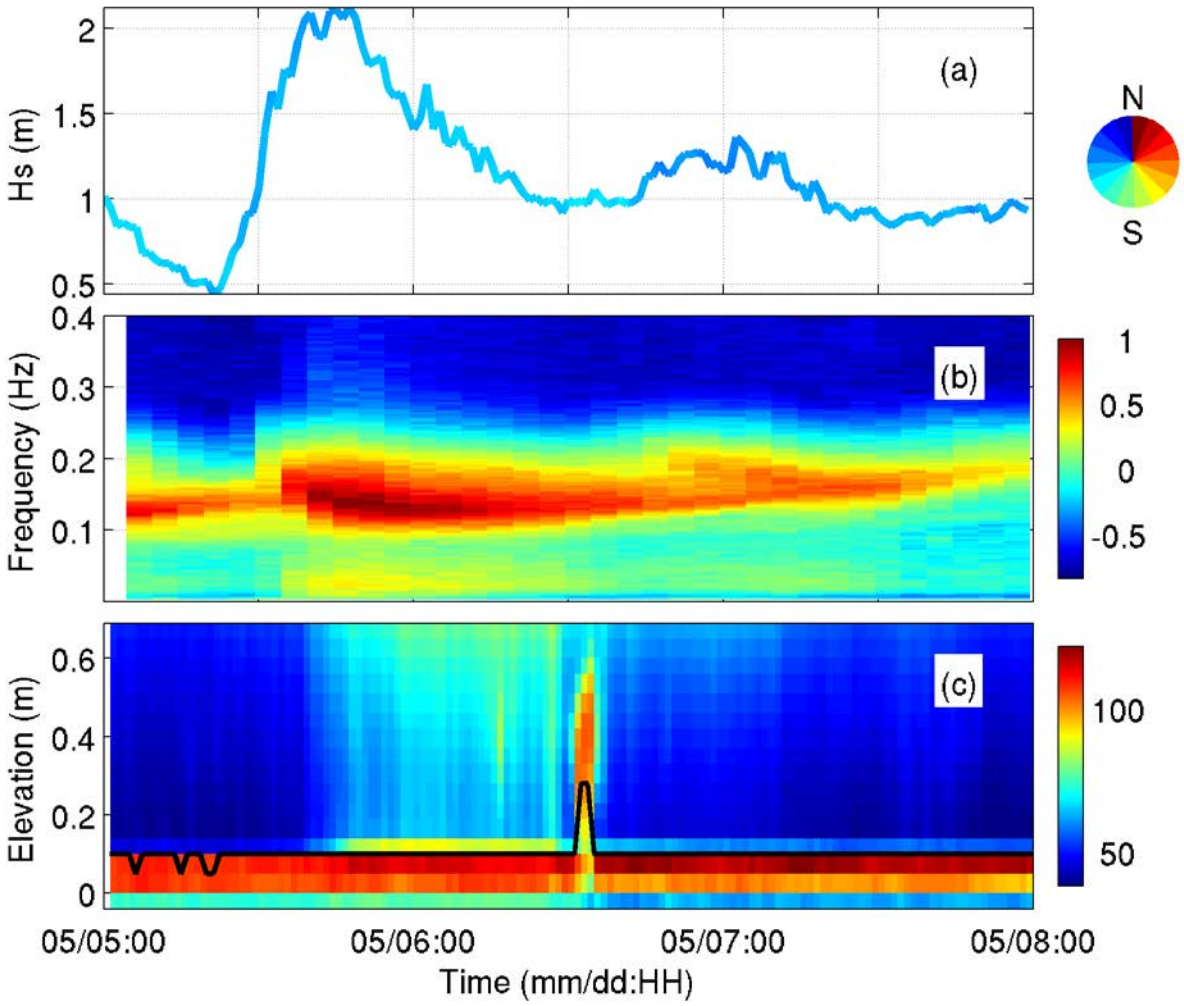

Figure 22. *Shown is significant wave height and direction (a) reported as coming from, mean b) free surface spectral density (b) estimated from pressure record, and acoustic backscatter intensity (counts) near the bed (c) with contour of maximum backscatter (solid black line) at the deep quadpod location.*

During the storm event, 5-6 May, no significant munitions mobility was observed at the deep quadpod location. However, both munitions mobility (Figure 23) and burial was observed at the shallow quadpod location. Mobility for the largest 155 mm surrogate and replica munitions, D6 and D3, respectively, was observed between 1400-2000 on 5 May. A time sequence of three sector scanning sonar images shown in Figure 24 highlights the initial positions of the munitions before the storm, after mobility, and subsequent burial. Burial begins around 2100 on 5 May and continues through 1200 on 6 May.

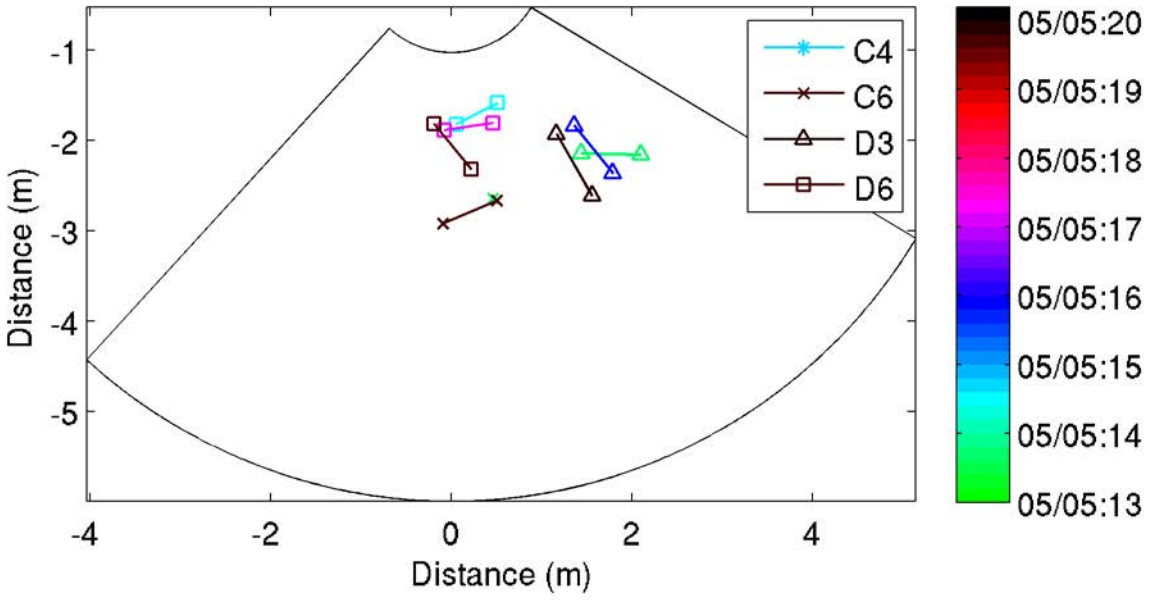

Figure 23. *Using sector scanning sonar images we tracked the positions for targets at the shallow quadpod location. The color of the symbol in the legend denotes the last time the target mobility was observed.*

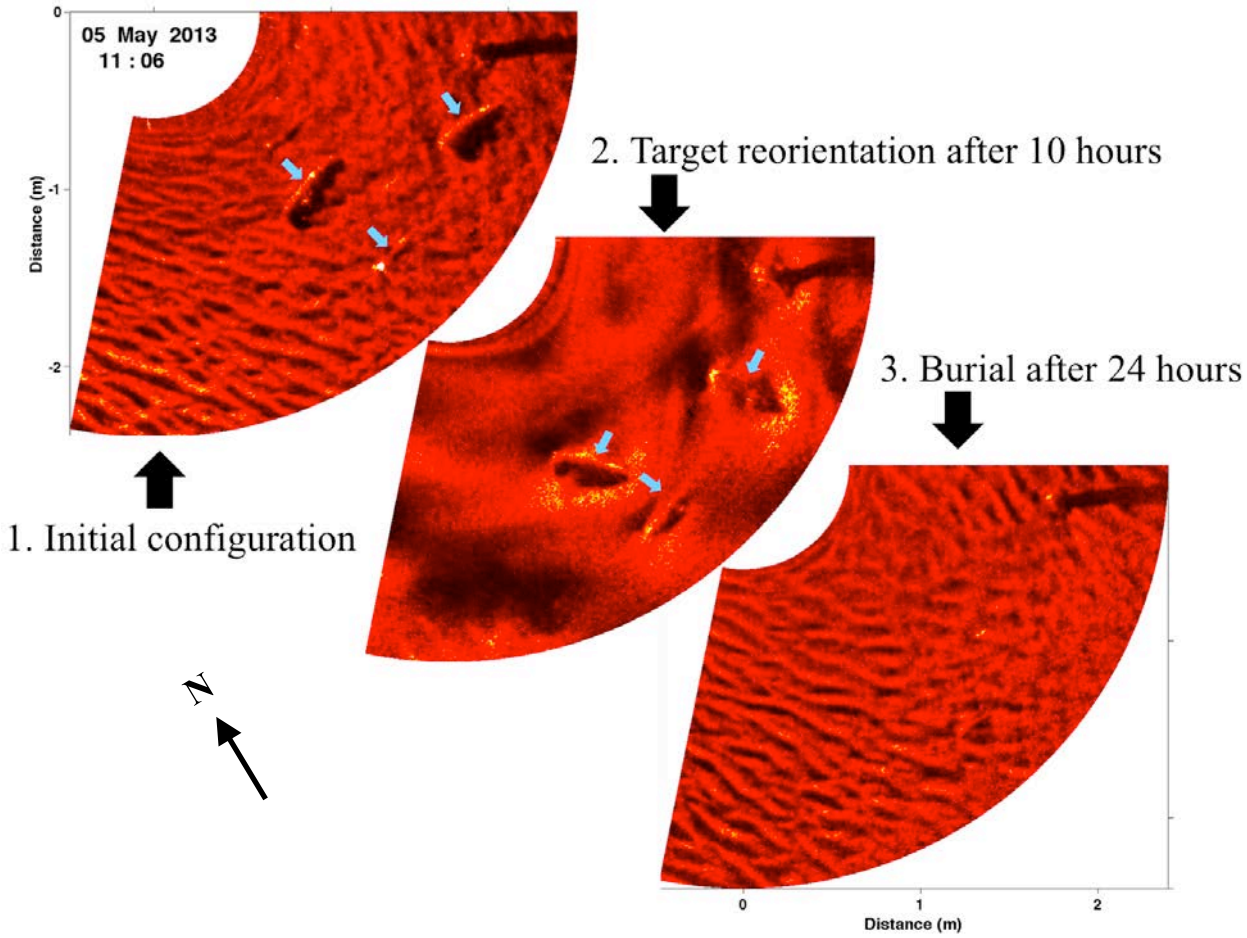

Figure 24. *Shown is a sequence of sector scanning sonar images highlighting the movement and burial of the largest targets at the shallow quadpod location. The initial positions of the largest targets are identified with the arrows (upper left). The same targets were still visible about 10 hours later in their new positions again indicated by arrows (center). The final image (lower right) was taken 24 hours later after the targets had been buried and sand ripples formed over the top of the freshly buried target field.*

3.2. Mechanisms for Munitions Mobility and Burial

During the high-energy wave event, 5-6 May, an estimated 15 cm of sediment was accreted at the shallow quadpod location and all targets were buried in place. The significant wave height peaked at approximately 2 m and with waves propagating roughly shore-normal (Figure 15). During this time interval the PC-ADP measured relatively weak mean currents near the bed with an atypical profile (non-logarithmic) including velocities amplified right at the estimated bed level or location of maximum ABS (Figure 25). Mean currents were also observed below the estimated bed level occurring between 2000-2200 on 5 May. The ABS of the PC-ADP also showed significant suspended sediment in the water column during the same time interval (Figure 26a). Co-located with the PC-ADP was a pair of ADVs stacked vertically with the position of the lower ADV approximately 10 cm from the initial at rest bed ($z = 0$). At approximately 0500 on 6 May, the burial of the lower ADV was apparent from the ABS signal (Figure 26b). The burial of the instrument was confirmed visually on the morning of 8 May

during the maintenance dive (Figure 27). The timing of the ADV burial from the ABS record is roughly consistent with burial observed in the sector scanning sonar image sequence (Figure 24). If we assume that the bed level estimated from the maximum ABS in the PC-ADP record around 0500 on 6 May is a new maximum bed level, it is clear that the previous maximum ABS of nearly 10 cm higher was not a true detection of bed level. Evidence from the pencil beam and sector scanning sonars confirm the later arrival of sediment accretion at the shallow quadpod location.

One possible explanation for the apparent false detection of the bed level using the location of the maximum ABS in the PC-ADP record is that the heightened wave conditions created a thick layer of mobile sediment confined near the bed (~15 cm). Such a sediment layer would also account for the observed near bed velocities that deviate from the typical logarithmic profile (Figure 25). Only a portion of the acoustic signal would be able to penetrate such a dense sediment layer. Consequently, the ABS observed by the PC-ADP inside this layer of sediment is low and the signal does not attenuate to the true bed level. The observed mobility of the largest 155 mm surrogate and replica also occurred during this time interval. One would only expect motion of these largest targets during very intense sediment transport conditions with a bedload (or sheet) layer on the order of the size of the object.

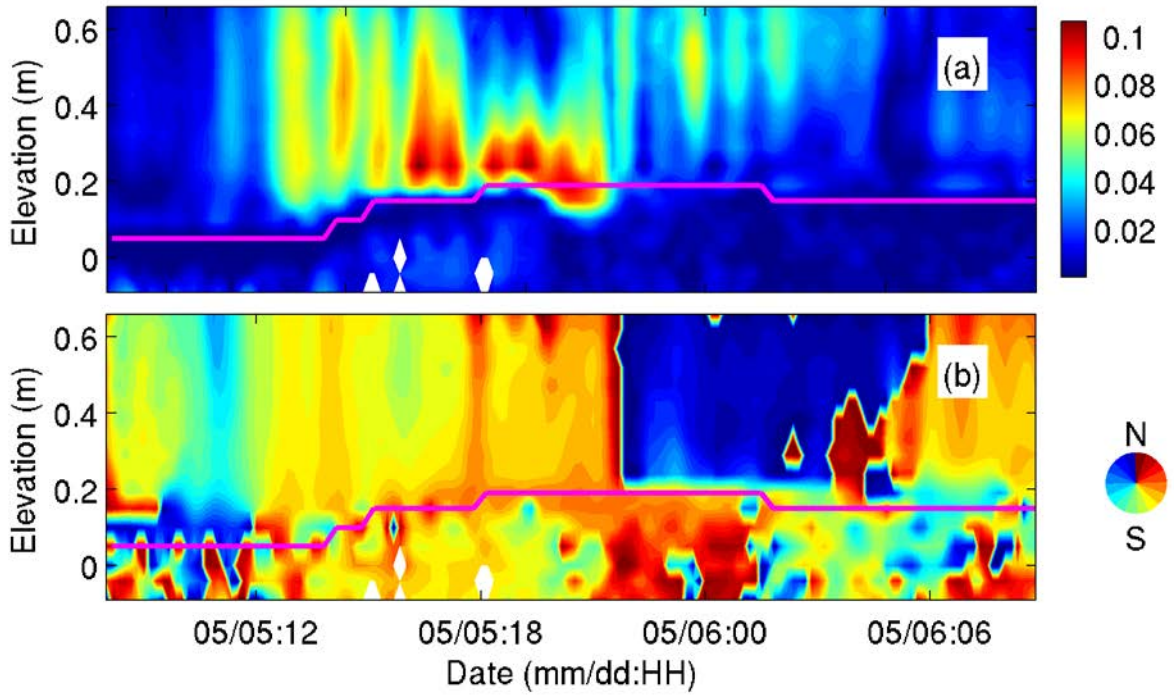

Figure 25. *Shown are mean currents (a) and direction (b) moving towards observed by the PC-ADP at the shallow quadpod location during the storm event on 5-6 May. The magenta line indicates the location of the maximum ABS.*

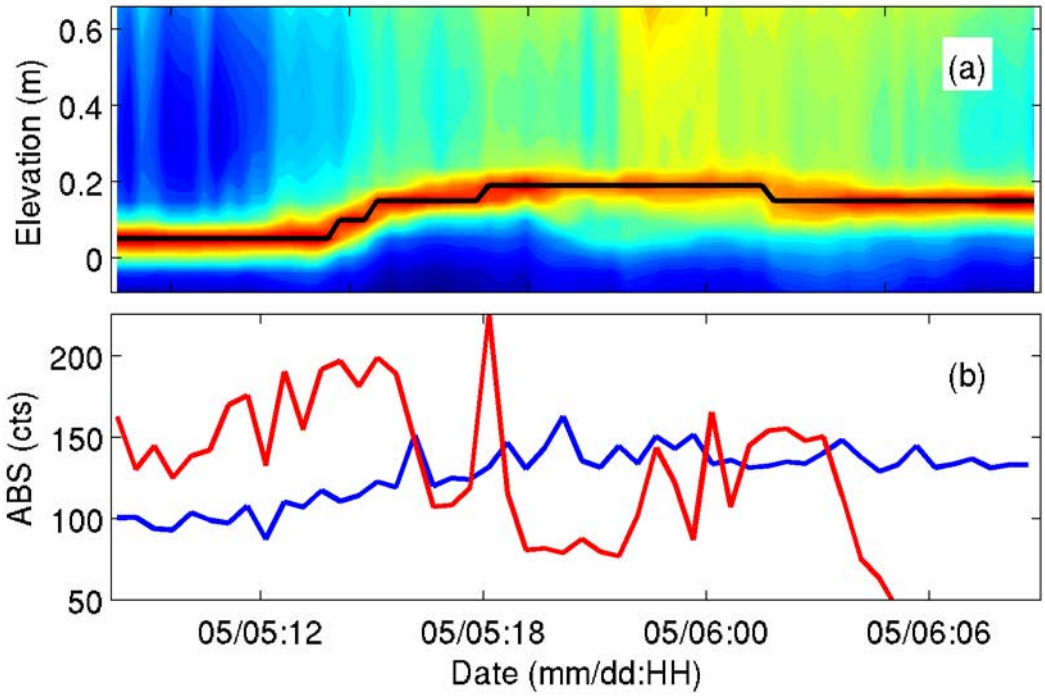

Figure 26. *Shown is the ABS in counts for the PC-ADP (a) and the ADVs (b) at the shallow quadpod location during the storm event on 5-6 May. The black line (a) indicates the location of the maximum ABS for the PC-ADP. The upper ADV (blue) and lower ADV (red) show intense ABS throughout the event with the signal in the lower ADV (red) dropping around 0500 on 6 May suggesting instrument burial.*

It is possible that a large bedform migrated near the shallow quadpod location and buried the target field (Figure 24) and the ADV (Figure 27). Unfortunately the bathymetric survey for TREX13 did not include the shallow quadpod location (Figure 7). The only direct evidence we have for such a bedform was shown in the diver photograph of the partially buried 155 mm replica (Figure 11). Preliminary analysis of bathymetric surveys performed at an adjacent location in slightly deeper water (>10 m) show the sparse existence of large bedforms (pers. comm. Christian de Moustier).

When comparing the storm of 5-6 May to the prior event on 4 May (see Figure 12), we observed that the energy in the swell frequency band ($0.5\,f_p \le f \le 1.5\,f_p$) is comparable at the peak of each event (Figure 28). However, during the storm event of 5-6 May there is additional energy in the infragravity band ($f \le 0.5\,f_p$) that raises the total energy of the event. When separating the cross shore and alongshore velocity components, the infragravity component dominates in the alongshore direction and suggests the presence of edge waves (Figure 29). Edge waves may be a potential mechanism for suspending sediment and enhancing the amount of sediment observed near the bed. The propagation of edge waves may also lead to the development, organization, and migration of large-scale bedforms.

Figure 27. *Diver photo taken on the morning of 8 May of the lower ADV of the vertically stacked pair partially buried. The ABS record from the ADV indicates that burial occurred around 0500 on 6 May.*

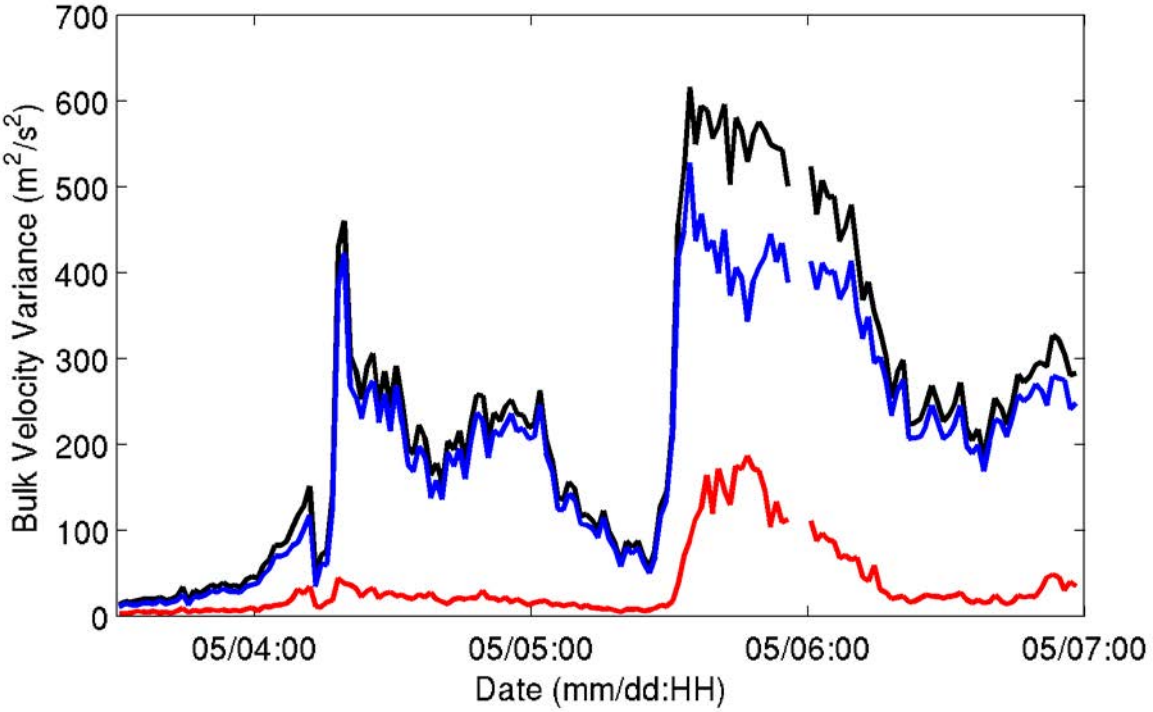

Figure 28. *Bulk velocity variance at the shallow quadpod location divided into spectral bands for infragravity frequencies (red) and swell frequencies (blue). Total shown in black.*

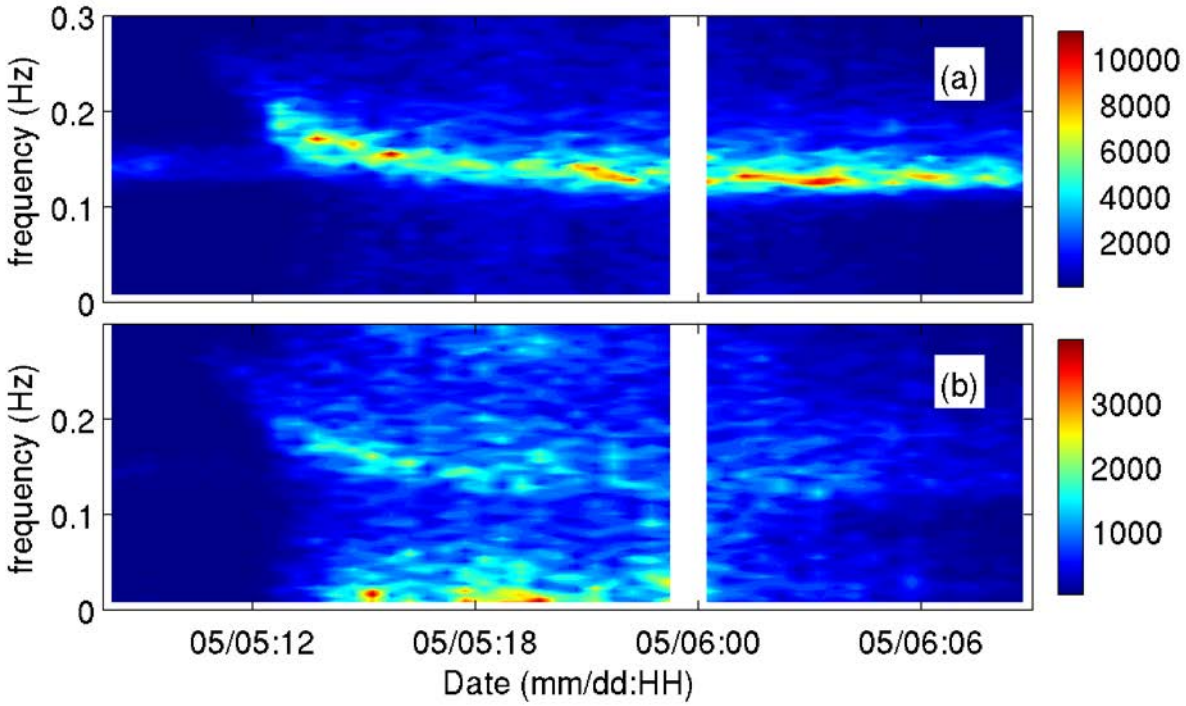

Figure 29. *Velocity spectral density measured approximately 80 cm above the bed in the cross-shore (a) and alongshore (b) directions.*

3.3. Sedimentology

Sediment samples were collected at both the shallow and deep quadpod locations. Diver push cores were collected during deployment at both locations (2 cores at each location). However, due to complications cores were only collected at the shallow quadpod location during the retrieval (2 additional cores for a total of 6). One of each of the two cores collected during the deployment and retrieval at shallow quadpod location has been analyzed; however, at the deep quadpod location detailed grain size analysis remains unfinished. Grain size distributions were obtained with standard sieve techniques and results for porosity, bulk density, and void ratio were obtained by measuring the weight loss or water weight (e.g., Jackson & Richardson, 2007). A summary of the cores collected and the status of the performed sediment analyses is found in Table 3.

The two cores analyzed at the shallow quadpod location are nearly 100% sand (Table 4). The remaining fraction is gravel sized shell hash found at the bottom of the core collected during the retrieval (16 – 20 cm deep). The samples taken from the deployment core (D1) were by mean, $\phi = 2.11$, which is a medium sand, but there was a well-sorted fine tail with 81% of the particles falling within the fine sand category. The surface layer extended to 8 cm, below which the grain distribution becomes more disperse and is moderately well sorted with increasing contributions of medium and coarse sand. It would appear that 8 cm depth is the base of the previously mobilized sand layer from a hydrodynamic event (e.g., winter storm) that occurred before the deployment. The remaining sediment deeper in the core was not analyzed for grain size. The samples taken from the retrieval core (R1) were by mean, $\phi = 2.14$, which is a medium sand, but there was a well-sorted fine tail with 79% of the particles falling within the fine sand category. The surface layer extended down to 14 cm, below which the grain distribution becomes enriched with medium sand grains and somewhat depleted in fine and very fine sand grains. The last 4 cm (10 – 14 cm) of the surface layer is the most homogeneous of the sediment intervals and represents the most intensely reworked sediments from the storm event (5-6 May) forming the base of the fluidized surficial layer. It is important to note that the estimated surface layer thickness of 14 cm is consistent with estimates for the deposition layer of 15 cm from the ADV and PC-ADP (Section 3.2). Below 14 cm there is slightly coarser sediments representing the lag layer from which finer particles were scavenged by winnowing apparent by the increased amount of gravel-sized shell hash deeper than 14 cm.

Quadpod Location	Deployment / Retrieval	Core #	Grain Size Analysis	Mass/Volume Analysis
shallow	deployment	D1	partial	complete
shallow	deployment	D2	partial	complete
shallow	retrieval	R1	complete	complete
shallow	retrieval	R2	complete	complete
deep	deployment	D3	none	partial
deep	deployment	D4	none	partial

Table 3. *Summary of cores collected and status of analyses.*

Depth Range (cm)	**% Gravel**		**% Sand**		**Mean ϕ**		**Standard Deviation ϕ**		**% Porosity**		**Bulk Density (g/cc)**		**Void Ratio (e)**	
Core #	D1	R1	D1	R1	D1	R1	D1	R1	D1	R1	D1	R1	D1	R1
0 – 2	0.00	0.04	100.00	99.96	2.14	2.06	0.39	0.40	38.35	39.55	2.04	2.02	0.62	0.65
2 – 4	0.00	0.00	100.00	100.00	2.12	2.04	0.40	0.40	39.28	40.14	2.03	2.02	0.65	0.67
4 – 6	0.00	0.02	100.00	99.98	2.13	2.08	0.42	0.46	39.13	38.96	2.03	2.03	0.64	0.64
6 – 8	0.02	0.01	99.98	99.99	2.23	2.21	0.43	0.44	38.84	39.46	2.04	2.03	0.63	0.65
8 – 10	0.13	0.01	99.87	99.99	1.94	2.24	0.62	0.40	37.62	39.26	2.06	2.03	0.60	0.65
10 – 12	–	0.00	–	100.00	–	2.22	–	0.37	38.17	39.95	2.05	2.02	0.62	0.67
12 – 14	–	0.02	–	99.98	–	2.22	–	0.40	38.60	40.40	2.04	2.01	0.63	0.68
14 – 16	–	0.03	–	99.97	–	2.15	–	0.45	37.05	40.29	2.07	2.01	0.59	0.67
16 – 18	–	0.10	–	99.90	–	2.11	–	0.47	38.00	40.90	2.05	2.00	0.61	0.69
18 – 20	–	0.23	–	99.77	–	2.08	–	0.45	–	39.19	–	2.03		0.64

Table 4. *Sediment properties from diver push cores taken during the deployment (D1) and the retrieval (R1) of the instrumentation at the shallow quadpod location.*

3.4. Sediment Transport

We have made preliminary estimates of sediment transport rates using wave data from the Nortek AWAC. Wave statistics were computed for every half-hour. Linear wave theory was used to estimate bottom velocities needed to drive engineering formulae to predict sediment transport rates. The bedload transport rate was estimated using the classic formula of Meyer-Peter and Muller (1948). The suspended load transport rate was estimated using an engineering formulation (Soulsby, 1997; van Rijn, 2007). The two time series for the magnitudes of the transport rates through the end of the storm event on 5-6 May are plotted in Figure 30. As expected for medium sand the suspended load transport dominates the bedload transport rate during the storm event. The peak magnitude of the total sediment transport rate estimated here was consistent (within 20%) of the magnitude for the total sediment transport rate estimated during the storm on 12 October 1990 at Duck, NC (Thornton et al., 1996). Coincidentally, the sediment characteristics were similar between the two sites (shallow quadpod location and Duck, NC), similar peak significant wave heights were observed (~ 2 m), and wave observations were performed in similar water depths (7 – 8 m). However, the sediment transport rates at the Duck field site were estimated using the classic energetics formulation (e.g., Bagnold, 1966; Bowen, 1980; Bailard, 1981).

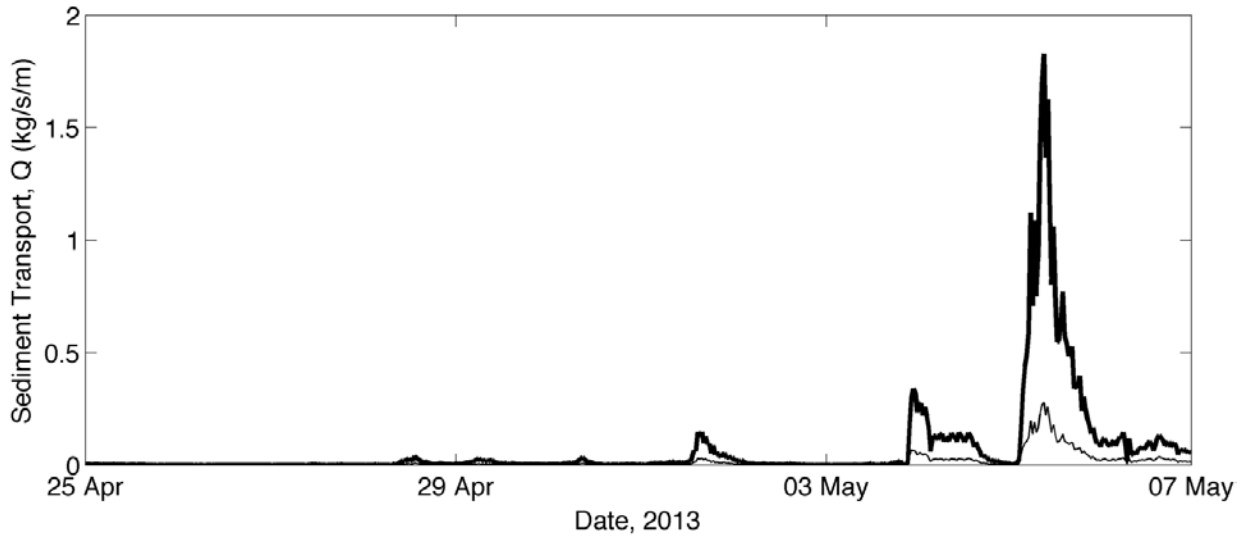

Figure 30. *Sediment transport rate, Q, for suspended load (heavy) and bedload (thin) plotted as a function of time through the storm event on 5-6 May.*

4. Conclusions to Date

Munitions mobility and burial for the largest surrogates and replicas deployed were observed at the shallow quadpod location in ~7.5 m water depth during the passage of an atmospheric front, 5 – 6 May 2013. During the same storm event, similar munitions mobility and sediment transport were not observed at the deep quadpod location in ~20 m water depth. The more surprising observation was the subsequent and rapid burial of all surrogate and replica munitions during a 24-hour period following the mobility at the shallow quadpod location. A maintenance dive was performed on the morning of 8 May 2013 after the storm event and found only one replica partially buried, which alerted us to the possibility that the other targets may have been buried in place. Divers were able to recover a total of 8 munitions buried at the shallow quadpod location by hand excavation.

The observed rapid burial of our target field at the shallow quadpod location provides a unique and challenging data set for ongoing modeling studies, particularly when coupled with the data sampled simultaneously at the deep quadpod location where limited mobility and no burial were observed. We believe we have sufficient data available that includes the munitions type along with the observed mobility, detailed hydrodynamic conditions (across the water column), and sediment characteristics and transport conditions at high temporal frequency to provide ongoing modeling studies with a unique and challenging benchmark data set.

The project is at a Go/No-Go decision point for the proposed field effort to take place during year 2 at the US Army Corps of Engineers Field Research Facility (FRF) in Duck, NC. The Go/No-Go decision criterion as stated in the project brief to the Scientific Advisory Board held on 24 October 2012 was to be "based on results from Year 1 experiment and feedback from ongoing modeling studies." We recommend continuing the project and performing the proposed year 2 field effort at the FRF in Duck, NC. The year 2 field effort is tentatively planned for the September-October 2014 time frame. Between now and the proposed field effort we will

continue analysis of the results from the year 1 field effort with particular emphasis placed on making our data available to ongoing modeling studies. We will participate in the planned SERDP workshop for modeling studies to be coordinated by the Munitions Response Program.

After consultation with ongoing modeling studies we will make any necessary adjustments to our data collection methods. We expect feedback from the ongoing modeling studies to provide guidance for the environments and types of data still needed for validation and simulation. One tremendous advantage for the data collection to be performed at the FRF in Duck, NC is the infrastructure provided by the FRF will allow for real time monitoring of our instrumentation and the target field. For example, if we had known a priori that targets were buried in place during the maintenance dive performed on 8 May 2013 we would have left the targets buried with the hope that future hydrodynamic conditions might lead to the observation of target excavation.

5. References

Bagnold, R.A., An approach to the sediment transport problem from general physics, *Geol. Surv. Prof. Pap. 422-I*, U.S. Dep. of the Interior, Washington, D.C., 1966.

Bailard, J.A., An energetics total load sediment transport model for a plane sloping beach, *J. Geophys. Res.*, *86*, 10,938-10,954, 1981.

Bowen, A.J., Simple models of nearshore sedimentation; beach profiles and longshore bars; in *The Coastline of Canada*, edited by S.B. McCann, *Pap. Geol. Surv. Can.*, *80-10*, 1-11, 1980.

Jackson, D.R., and M.D. Richardson, *High-Frequency Seafloor Acoustics*, 616 pp., Springer, New York, NY, 2007.

Meyer-Peter, E., and R. Muller, Formulas for bed-load transport, *Proc. Int. Ass. Hydr. Struct. Res.*, Stockholm, 1948.

Soulsby, R., *Dynamics of marine sands,* Thomas Telford, London, 1997.

Thorton, E.B., R.T. Humiston, and W. Birkemeier, Bar/trough generation on a natural beach, *J. Geophys. Res.*, *101*(C5), 12,097-12,110, 1996.

van Rijn, L.C., Unified View of Sediment Transport by Currents and Waves. II: Suspended Transport, *J. Hydraul. Eng., 133*(6), 668–689, 2007.